Astronomy & Astrophysics manuscript no. astro-ph
October 5, 2009

Chemical abundance analysis of the Open Clusters Cr 110, NGC 2099 (M 37), NGC 2420, NGC 7789 and M 67 (NGC 2682) ⋆

E. Pancino[1], R. Carrera[1,2], E. Rossetti[1], and C. Gallart[2]

[1] INAF – Osservatorio Astronomico di Bologna, via Ranzani 1, I-40127 Bologna, Italy
e-mail: elena.pancino@oabo.inaf.it, emanuel.rossetti@oabo.inaf.it, ricardo.carrera@oabo.inaf.it
[2] Instituto de Astrofisica de Canarias, via Lactea s/n, E-38200, La Laguna, Tenerife, Spain
e-mail: rcarrera@iac.es,carme@iac.es

Received July 24, 2009; accepted October 2, 2009

ABSTRACT

Context. The present number of Galactic Open Clusters that have high resolution abundance determinations, not only of [Fe/H], but also of other key elements, is largely insufficient to enable a clear modeling of the Galactic Disk chemical evolution.
Aims. To increase the number of Galactic Open Clusters with high quality measurements.
Methods. We obtained high resolution (R∼30 000), high quality (S/N∼50-100 per pixel), echelle spectra with the fiber spectrograph FOCES, at Calar Alto, Spain, for three red clump stars in each of five Open Clusters. We used the classical Equivalent Width analysis method to obtain accurate abundances of sixteen elements: Al, Ba, Ca, Co, Cr, Fe, La, Mg, Na, Nd, Ni, Sc, Si, Ti, V, Y. We also derived the oxygen abundance through spectral synthesis of the 6300 Å forbidden line.
Results. Three of the clusters were never studied previously with high resolution spectroscopy: we found [Fe/H]=+0.03±0.02 (±0.10) dex for Cr 110; [Fe/H]=+0.01±0.05 (±0.10) dex for NGC 2099 (M 37) and [Fe/H]=–0.05±0.03 (±0.10) dex for NGC 2420. This last finding is higher than typical recent literature estimates by 0.2–0.3 dex approximately and in better agreement with Galactic trends. For the remaining clusters, we find: [Fe/H]=+0.05±0.02 (±0.10) dex for M 67 and [Fe/H]=+0.04±0.07 (±0.10) dex for NGC 7789 . Accurate (to ∼0.5 km s^{-1}) radial velocities were measured for all targets, and we provide the first high resolution based velocity estimate for Cr 110, $<V_r>$=41.0±3.8 km s^{-1}.
Conclusions. With our analysis of the new clusters Cr 110, NGC 2099 and NGC 2420, we increase the sample of clusters with high resolution based abundances by 5%. All our programme stars show abundance patterns which are typical of open clusters, very close to solar with few exceptions. This is true for all the iron-peak and s-process elements considered, and no significant α-enhancement is found. Also, no significant sign of (anti-)correlations for Na, Al, Mg and O abundances is found. If anticorrelations are present, the involved spreads must be <0.2 dex. We then compile high resolution data of 57 OC from the literature and we find a gradient of [Fe/H] with Galactocentric Radius of –0.06±0.02 dex kpc^{-1}, in agreement with past work and with Cepheids and B stars in the same range. A change of slope is seen outside R_{GC}=12 kpc and [α/Fe] shows a tendency of increasing with R_{GC}. We also confirm the absence of a significant Age-Metallicity relation, finding slopes of –2.6±1.1 10^{-11} dex Gyr^{-1} and 1.1±5.0 10^{-11} dex Gyr^{-1} for [Fe/H] and [α/Fe] respectively.

Key words. Stars: abundances – Galaxy: disk – Galaxy: open clusters and associations: individual: Cr 110; NGC 2099; NGC 2420; M 67; NGC 7789

1. Introduction

Open clusters (hereafter OC) are the ideal *test particles* in the study of the Galactic disk, providing chemical and kinematical information in different locations and at different times. Compared to field stars, they have the obvious advantage of being coeval groups of stars, at the same distance and with a homogeneous composition. Therefore, their properties can be determined with smaller uncertainties. Several attempts have been done in the past to derive two fundamental relations using OC: the *metallicity gradient* along the disk and the *age-metallicity relation* (hereafter AMR) of the disk (e.g. Janes, 1979; Panagia & Tosi, 1980; Twarog et al., 1997; Friel et al., 2002; Chen et al., 2003; Salaris et al., 2004), but they were hampered by the lack of large and homogeneous high quality datasets.

In particular, the lack of a *metallicity scale* extending to solar metallicity with comparable precision to the lower metallicity regimes (i.e., Zinn & West, 1984; Carretta & Gratton, 1997) represents the main problem from the point of view of *(i)* the study of the Galactic disk; *(ii)* tests of stellar evolution models for younger and more metal-rich *simple stellar populations* and *(iii)* the use of those stellar populations as templates for extragalactic studies of population synthesis. Of the ∼1700 known OC (Dias et al., 2002, and updates), only a subset of ∼140, i.e., 8% of the total, possesses some metallicity determination. Most of these have been obtained through different photometric studies in the Washington (e.g. Geisler et al., 1991, 1992), DDO (e.g. Clariá et al., 1999), Strömgren (e.g. Bruntt et al., 1999; Twarog et al., 2003), UBV (e.g. Cameron, 1985) and IR (e.g. Tiede et al., 1997) photometric systems and passbands, giving often rise to considerable differences with those obtained from spectroscopy (see Gratton, 2000, and references therein).

Send offprint requests to: E. Pancino

⋆ Based on data collected with the fiber spectrograph FOCES at the 2.2m Calar Alto Telescope. Also based on data from the 2MASS survey and the WEBDA, VALD, NIST and GEISA online databases.

Table 1. Observing Logs and Programme Stars Information.

Cluster	Star	α_{J2000} (hrs)	δ_{J2000} (deg)	B (mag)	V (mag)	I_C (mag)	R (mag)	K_S (mag)	n_{exp}	$t_{exp}^{(tot)}$ (sec)	S/N(≃6000Å)
Cr 110[a]	2108	06:38:52.5	+02:01:58.4	14.79	13.35	—	—	9.76	6	16200	70
	2129	06:38:41.1	+02:01:05.5	15.00	13.66	12.17	12.94	10.29	7	18900	70
	3144	06:38:30.3	+02:03:03.0	14.80	13.49	12.04	12.72	10.19	6	16195	65
NGC 2099 (M 37)[b]	067	05:52:16.6	+32:34:45.6	12.38	11.12	9.87	—	8.17	3	3600	95
	148	05:52:08.1	+32:30:33.1	12.36	11.09	—	—	8.05	3	3600	105
	508	05:52:33.2	+32:27:43.5	12.24	10.98	—	—	7.92	3	3900	85
NGC 2420[c]	041	07:38:06.2	+21:36:54.7	13.75	12.67	11.61	12.13	10.13	5	9000	70
	076	07:38:15.5	+21:38:01.8	13.65	12.66	11.65	12.14	10.31	5	9000	75
	174	07:38:26.9	+21:38:24.8	13.41	12.40	—	—	9.98	5	9000	60
NGC 2682 (M 67)[d]	0141	08:51:22.8	+11:48:01.7	11.59	10.48	9.40	9.92	7.92	3	2700	85
	0223	08:51:43.9	+11:56:42.3	11.68	10.58	9.50	10.02	8.00	3	2700	85
	0286	08:52:18.6	+11:44:26.3	11.53	10.47	9.43	9.93	7.92	3	2700	105
NGC 7789[e]	5237	23:56:50.6	+56:49:20.9	13.92	12.81	11.52	—	9.89	5	9000	70
	7840	23:57:19.3	+56:40:51.5	14.03	12.82	11.49	—	9.83	6	9000	75
	8556	23:57:27.6	+56:45:39.2	14.18	12.97	11.65	—	10.03	3	5400	45

[a] Star names and I_C & R magnitudes from Dawson & Ianna (1998); coordinates and B & V magnitudes from Bragaglia & Tosi (2003); K_S magnitudes from 2MASS

[b] Star names from van Zeipel & Lindgren (1921); coordinates from Kiss et al. (2001); B & V magnitudes from Kalirai et al. (2001); I_C magnitudes from Nilakshi & Sagar (2002); K_S magnitudes from 2MASS

[c] Star names from Cannon & Lloyd (1970); coordinates from Stetson (2000) and Lasker et al. (1990); B & V magnitudes from Anthony-Twarog et al. (1990); I_C & R magnitudes from Stetson (2000); K_S magnitudes from 2MASS

[d] Star names from Fagerholm (1906); coordinates from Fan et al. (1996); B, V & I_C magnitudes from Sandquist (2004); B magnitude for star 286 and R magnitudes from Janes & Smith (1984); K_S magnitudes from 2MASS

[e] Star names and V & I_c magnitudes from Gim et al. (1998a); J1950 coordinates from Kustner (1923), precessed to J2000; B magnitudes from Mochejska & Kaluzny (1999); K_S magnitudes from 2MASS

In a much smaller number of clusters, abundances have been derived from low-resolution spectroscopy (e.g., Carrera et al., 2007; Warren & Cole, 2008), with admirable attempts to obtain large and homogeneous datasets (see Friel & Janes, 1993; Friel et al., 2002), in spite of the non-negligible uncertainties involved in the procedure.

A few research groups (see Section 6 for more details) are presently obtaining high quality spectra and are producing more precise abundance determinations. The study of elements other than the iron-peak ones (such as α, s- and r-process, light elements), allows one to put more constraints on the sites of production of those elements (SNe Ia, SNe II, giants and supergiants, Wolf-Rayet stars), and therefore on their production timescales. These are fundamental ingredients for the chemical evolution modeling of the Galactic Disk (Tosi, 1982; Chiappini et al., 2001; Colavitti et al., 2009).

For these reasons, we obtained high resolution spectra for a sample of poorly studied old OC. We present here the detailed abundance analysis of five clusters observed during our first run at Calar Alto. Observations and data reductions are described in Section 2; the linelist and equivalent width measurements are detailed in Section 3 while the abundance analysis methods and results are presented in Section 4; abundance results are then discussed and compared with literature results in Sections 5, 6 and 7; finally, we summarize our results and draw our conclusions in Section 8.

2. Observational Material

Three red clump stars[1] were selected in each of the target clusters using the WEBDA[2] database (Mermilliod, 1995) and the 2MASS[3] survey data for the infrared K_S magnitudes (Skrutskie et al., 2006). More details on references for star names, coordinates and magnitudes can be found in Table 1, while the position of our targets in the Color Magnitude Diagrams (CMDs) obtained from WEBDA are shown in Figure 1.

Observations were done between the 1st and 10th of January 2004 with the fiber echelle spectrograph FOCES at the 2.2 m Calar Alto Telescope, in Spain. The sky was generally clear, though a few nights had thin cirrus and sometimes clouds, forcing us to increase the exposure times considerably. All stars were observed in 3–16 exposures lasting 15–90 min each, depending on the magnitude, until a global S/N ratio between 70 and 100 (per pixel) was reached around 6000 Å (Table 1). Each night we took a sky exposure lasting as the longest one of the night. The sky level was negligible for all exposures with S/N>20, therefore exposures with S/N<20 were neglected and we did not subtract the sky, to avoid adding noise to the spectra. Sky emission lines, even in the red part of the spectrum, did only occasionally disturb

[1] Though fainter than the brigthest giants, red clump stars have the advantage of a higher gravity and temperature, that reduces considerably line crowding. Also, clump stars are easy to identify even in the sparsest cluster, maximizing the chance of choosing cluster members.

[2] `http://www.univie.ac.at/webda`

[3] `http://www.ipac.caltech.edu/2mass`. 2MASS (Two Micron All Sky Survey) is a joint project of the University of Massachusetts and the Infrared Processing and Analysis Center/California Institute of Technology, funded by the National Aeronautics and Space Administration and the National Science Foundation.

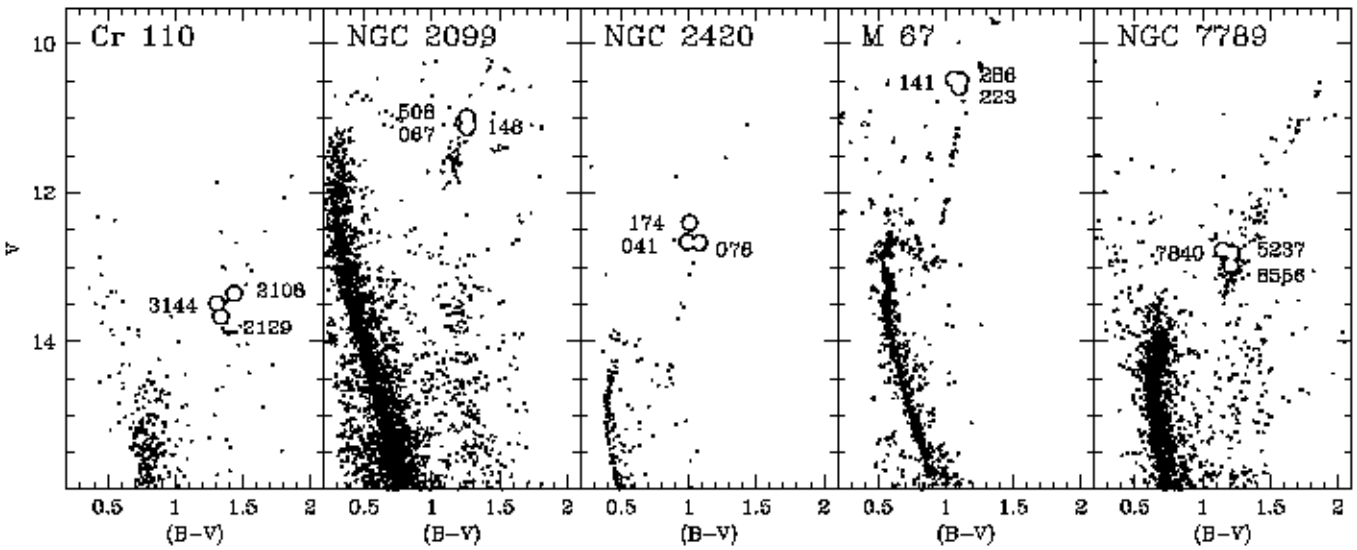

Fig. 1. V, (B–V) Color Magnitude Diagrams of the programme clusters (from the WEBDA), with the location of our target stars.

the measurements of some absorption lines, that were discarded. The spectral resolution was $R \simeq 30\,000$ for all spectra.

2.1. Data Reductions

Data reductions were done with IRAF[4] within the *imred* and *echelle* packages. The following steps were performed: bias subtraction, flatfielding, order tracing with optimal extraction, background subtraction, wavelength calibration with the help of a Thorium-Argon lamp, and final merging (and rebinning) of overlapping orders. The one-dimensional spectra obtained from different exposures (with S/N>20) were median-averaged to produce one single high S/N spectrum for each star, used for equivalent width measurements (Section 3.3). Finally, the noisy ends of each combined spectrum were cut, allowing for an effective wavelength coverage from 5000 to 9000 Å.

Sky absorption lines (telluric bands of O_2 and H_2O) were removed using the IRAF task *telluric* with the help of two hot, rapidly rotating stars, HR 3982 and HR 8762, chosen from the *Bright Star Catalogue* (Hoffleit & Jaschek, 1991). HR 3982 and HR 8762 were observed each night at an airmass not too different from the scientific targets. Residuals of the correction in the red part of the spectrum (for example from the strong O_2 band around 7600 Å) prevented us from using most of the corresponding spectral regions for our abundance analysis. Also, after 8400 Å, the echelle orders do not overlap anymore and small gaps appear.

2.2. Radial Velocities

Radial velocities were measured with the help of DAOSPEC (Stetson & Pancino, 2008, see also Section 3.3). Measurements were based on ≃360 absorption lines of different elements (see Section 3) with typical measurement errors on the mean of about 0.1 km s^{-1}. All measurements were performed separately on the one-dimensional spectra extracted from the single exposures for each star, including those with S/N<20, that were not used for the abundance analysis. In this way, we could check that no significant radial velocity variations were present.

[4] Image Reduction and Analysis Facility. IRAF is distributed by the National Optical Astronomy Observatories, which is operated by the association of Universities for Research in Astronomy, Inc., under contract with the National Science Foundation

Table 2. Heliocentric radial velocities measurements and 1σ errors $(V_r \pm \delta V_r)_{here}$ for each programme star. Literature measurements, when available, are also reported with their uncertainties $(V_r \pm \delta V_r)_{lit}$.

Cluster	Star	$(V_r \pm \delta V_r)_{here}$ (km s^{-1})	$(V_r \pm \sigma V_r)_{lit}$ (km s^{-1})
Cr 110	2108	44.47 ± 0.54	45 ± 8[a]
	2129	38.74 ± 0.64	45 ± 8[a]
	3144	37.81 ± 0.69	45 ± 8[a]
NGC 2099 (M 37)	067	8.79 ± 0.10	8.04 ± 0.19[b]
	148	9.05 ± 0.36	8.73 ± 0.19[b]
	508	9.40 ± 0.28	8.96 ± 0.19[b]
NGC 2420	041	74.23 ± 0.87	79.0 ± 4.2[c]
	076	75.49 ± 0.41	75.7 ± 8.6[c]
	174	73.66 ± 1.17	68.0 ± 0.9[c]
NGC 2682 (M 67)	141	35.23 ± 0.05	33.5 ± 2.3[d]
	223	34.92 ± 0.31	33.0 ± 1.1[d]
	286	38.90 ± 0.46	33.2 ± 2.0[d]
NGC 7789	5237	–51.06 ± 0.99	–57.17 ± 0.23[e]
	7840	–49.06 ± 0.81	–49.21 ± 0.28[e]
	8556	–53.37 ± 0.81	–54.10 ± 0.32[e]

[a] Cluster average by Carrera et al. (2007), based on 8 stars.
[b] Mermilliod et al. (2008), superseding Mermilliod et al. (1996).
[c] Average of measurements by Liu & Janes (1987), Friel et al. (1989) and Scott et al. (1995).
[d] Average of measurements by Mathieu et al. (1986), Pilachowski et al. (1988), Friel et al. (1989), Friel & Janes (1993), Suntzeff et al. (1992), Scott et al. (1995), Melo et al. (2001), Yong et al. (2005), Yadav et al. (2008).
[e] Gim et al. (1998b).

Table 3. Stellar Parameters for the programme stars.

Cluster	Star	$T_{\rm eff}^{(phot)}$ (K)	$T_{\rm eff}^{(spec)}$ (K)	$\log g^{(phot)}$ (cgs)	$\log g^{(spec)}$ (cgs)	$v_t^{(phot)}$ (km s^{-1})	$v_t^{(spec)}$ (km s^{-1})	M_{clump} ($M_\odot$)
Cr 110	2108	4914±111	4650	2.32±0.16	2.8	1.20±0.02/1.62±0.04	1.4	1.9±0.1
	2129	5056±223	4950	2.53±0.19	2.7	1.17±0.02/1.52±0.06	1.4	1.9±0.1
	3144	5112±258	4800	2.49±0.20	2.8	1.18±0.02/1.49±0.08	1.3	1.9±0.1
NGC 2099 (M 37)	067	4773±119	4550	2.15±0.32	2.7	1.22±0.03/1.68±0.05	1.5	2.7±0.2
	148	4708±116	4550	2.10±0.31	2.7	1.28±0.03/1.72±0.04	1.5	2.7±0.2
	508	4715±115	4500	2.05±0.32	2.8	1.23±0.03/1.72±0.04	1.5	2.7±0.2
NGC 2420	041	4616±77	4850	2.43±0.06	2.6	1.19±0.01/1.76±0.03	1.4	1.4±0.1
	076	4755±103	4800	2.51±0.06	2.6	1.18±0.01/1.69±0.03	1.6	1.4±0.1
	174	4730±77	4800	2.39±0.05	2.6	1.19±0.01/1.71±0.03	1.5	1.4±0.1
NGC 2682 (M 67)	141	4590±100	4650	2.42±0.04	2.8	1.19±0.01/1.78±0.04	1.3	1.3±0.1
	223	4594±100	4800	2.46±0.04	2.8	1.18±0.00/1.78±0.04	1.3	1.3±0.1
	286	4653±103	4850	2.45±0.04	2.8	1.18±0.01/1.75±0.04	1.4	1.3±0.1
NGC 7789	5237	4868±168	4900	2.53±0.15	2.8	1.17±0.02/1.63±0.04	1.2	1.8±0.1
	7840	4759±131	4800	2.47±0.15	2.7	1.18±0.02/1.69±0.04	1.5	1.8±0.1
	8556	4775±135	4900	2.54±0.15	2.9	1.17±0.02/1.68±0.04	1.4	1.8±0.1

Heliocentric corrections were computed with the IRAF task *rvcor*, which bears a negligible uncertainty of less than 0.005 km s^{-1}. Since we did not observe any radial velocity standard and our calibration lamps were not taken simultaneously, we used telluric absorption lines to find the absolute zero point of our radial velocity measurements. In particular, laboratory wavelengths of the H_2O absorption bands around 5800, 6500, 7000, 7200, 8000 and 8900 Å and of the O_2 absorption bands around 6300, 6900 and 7600 Å were obtained from the GEISA[5] database (Jacquinet-Husson et al., 1999, 2005) and we measured their radial velocity in our programme stars. The resulting zero-point corrections, based on 200–250 telluric lines, amount generally to no more than ±1 km s^{-1} with typical errors on the mean of about 0.5 km s^{-1}, approximately five times larger than those on the radial velocity measurements.

After applying the above corrections, and propagating the corresponding uncertainties, we computed a weighted average of the heliocentric velocities estimates for each exposure (see Table 2). All the programme stars appear to be radial velocity members of the observed clusters, with the possible exception of star 2108 in Cr 110, that has a slightly higher velocity than 2129 and 3144. However, since the value for 2108 is within 3σ from the mean value for the cluster, we decided not to reject this star. We can provide the first radial velocity estimate based on high resolution for Cr 110: $<V_r>$=41.0±3.8 km s^{-1}. Our determinations are generally in good agreement with literature values within 3σ, except maybe for star 5237 in NGC 7789, which is marginally dicrepant with the estimate by Gim et al. (1998b). However, there is perfect agreement between the two studies for the other two stars of NGC 7789, and our estimate appears more in line with a membership of 5237. In conclusion, we considered all the programme stars as likely radial velocity members of their respective clusters.

[5] http://ara.lmd.polytechnique.fr/htdOC-public/products/GEISA/HTML-GEISA/

2.3. Photometric Parameters

We first computed the dereddened colors[6] $(B–V)_0$, $(V–I_C)_0$[7] and $(V–K_TCS)_0$[8]. The adopted E(B–V) values are indicated in Table 4, where E(V–I_C) was obtained with the reddening laws by Dean et al. (1978), and E(V–K_TCS) with Cardelli et al. (1989). We were then able to obtain $T_{\rm eff}$ and the bolometric correction BC_V for each programme star, using both the Alonso et al. (1999) and the (theoretical and empyrical) Montegriffo et al. (1998) color-temperature relations, taking into account the uncertainties on magnitudes and reddening estimates. The average difference between the Alonso et al. (1999) and the Montegriffo et al. (1998) temperatures was $\Delta T_{\rm eff}$=178±66 K (for the empyrical calibration of Montegriffo et al., 1998) and $\Delta T_{\rm eff}$=127±69 K (for the theoretical calibration of Montegriffo et al., 1998). We averaged all the above $T_{\rm eff}$ estimates to obtain our photometric reference values with their 1σ uncertainties (Table 3).

Gravities were obtained from $T_{\rm eff}$ and BC_V using the fundamental relations

$$\log\frac{g}{g_\odot} = \log\frac{M}{M_\odot} + 2\log\frac{R_\odot}{R}$$

$$0.4(M_{\rm bol} - M_{\rm bol,\odot}) = -4\log\frac{T_{\rm eff}}{T_{\rm eff,\odot}} + 2\log\frac{R_\odot}{R}$$

where red clump masses were derived using Table 1 of Girardi & Salaris (2001), and are also shown in Table 3. We assumed $\log g_\odot$ = 4.437, $T_{\rm eff,\odot}$ = 5770 K and $M_{\rm bol,\odot}$ = 4.75, in conformity with the IAU recommendations (Andersen, 1999). The difference between the Alonso et al. (1999) and the (empyrical and theoretical, respectively) Montegriffo et al. (1998) estimates was $\Delta\log g$=0.20±0.13 and $\Delta\log g$=0.18±0.13. As above, we averaged all our estimats to obtain photometric gravities $\log g^{(phot)}$ (Table 3) and their 1σ uncertainties.

Finally, a photometric estimate of the microturbulent velocities v_t was obtained using both the prescriptions of

[6] Since R magnitudes are available for less than half of our sample, we decided to ignore them in the following.

[7] After dereddening, $(V–I_C)$ was also converted into $(V–I_J)$ using the prescription by Bessell (1979), to be used with the color-temperature relations by Alonso et al. (1999).

[8] We computed the K_TCS magnitudes from the 2MASS TCS magnitudes using the prescription by Kinman & Castelli (2002).

Table 4. Input cluster parameters.

Cluster	E(B–V) (mag)	(m-M)$_V$ (mag)	log Age (dex)
Cr 110[a]	0.54±0.03	13.37±0.38	9.23±0.15
NGC 2099 (M 37)[b]	0.27±0.04	11.53±0.19	8.61±0.16
NGC 2420[c]	0.04±0.03	11.88±0.27	9.47±0.17
NGC 2682 (M 67)[d]	0.04±0.02	9.67±0.11	9.64±0.05
NGC 7789[e]	0.27±0.04	12.23±0.20	9.21±0.12

[a] Averages of measurements by Tsarevskii & Abakumov (1971), Dawson & Ianna (1998) and Bragaglia & Tosi (2006).

[b] Averages of measurements by West (1967a), Jennens & Helfer (1975), Lyngå (1987), Mermilliod et al. (1996), Twarog et al. (1997), Kiss et al. (2001), Kalirai et al. (2001), Nilakshi & Sagar (2002), Grocholski & Sarajedini (2003), Bragaglia & Tosi (2006) and Hartman et al. (2008).

[c] Averages of measurements by McClure et al. (1974), Barbaro & Pigatto (1984), Vandenberg (1985), Lyngå (1987), Anthony-Twarog et al. (1990), Carraro & Chiosi (1994), Demarque et al. (1994), Twarog et al. (1997), Tadross et al. (2002) and Grocholski & Sarajedini (2003).

[d] Averages of measurements by Racine (1971), Barbaro & Pigatto (1984), Vandenberg (1985), Nissen et al. (1987), Hobbs & Thorburn (1991), Gilliland & Brown (1992), Demarque et al. (1992), Meynet et al. (1993), Montgomery et al. (1993), Carraro & Chiosi (1994), Dinescu et al. (1995), Fan et al. (1996), Twarog et al. (1997), Sarajedini (1999), Tadross et al. (2002), Grocholski & Sarajedini (2003), VandenBerg & Clem (2003), Laugalys et al. (2004) and Sandquist (2004).

[e] Averages of measurements by Burbidge & Sandage (1958), Arp (1962), Strom & Strom (1970), Jennens & Helfer (1975), Janes (1977), Claria (1979), Twarog & Tyson (1985), Lyngå (1987), Mazzei & Pigatto (1988), Friel & Janes (1993), Martinez Roger et al. (1994), Janes & Phelps (1994), Twarog et al. (1997), Gim et al. (1998b), Sarajedini (1999), Vallenari et al. (2000), Tadross et al. (2002) and Bartašiutė & Tautvaišienė (2004).

Ramírez & Cohen (2003), $v_t = 4.08 - 5.01\ 10^{-4}\ T_{\rm eff}$, and of Carretta et al. (2004), $v_t = 1.5 - 0.13\ \log g$. The latter takes into account the systematic effect discussed by Magain (1984) and is on average lower by $\Delta v_t = 0.49 \pm 0.08$ km s $^{-1}$ than the one by Ramírez & Cohen (2003). However, the actual amount of the correction for the Magain (1984) effect depends heavily on the data quality (i.e., resolution, S/N ratio, number of lines used, log gf values etc.). Therefore we chose not to average the two estimates, but to use them as an indication of the (wide) v_t range to explore in our abundance analysis (see Section 4.1).

3. Linelist, Atomic Data and Equivalent Widths

We created a masterlist of absorption lines by visually comparing our spectra with the the UVES solar spectrum[9] in the range 5000–9000 Å, and with the line lists extracted from the VALD[10] database (Kupka et al., 1999) and the Moore[11] (Moore et al., 1966) solar atlas. The masterlist was fed to DAOSPEC and EW were measured for all our programme stars. A first selection was applied to reject all those lines that were measured in 10 stars or less (out of 15) and that had EW systematically larger than 250 mÅ. Later, after performing a first crude abundance analysis (see Section 4.1), we rejected all the lines that gave sistematically discrepant abundances, especially if the formal DAOSPEC relative error (δEW/EW, Figure 2) was around 15% or more, and the DAOSPEC quality parameter was above 1.5 (for more details about DAOSPEC error and quality parameter, see Section 3.3). The final linelist, including atomic data and EW measurements for all programme stars, contains 358 absorption lines of 17 species, and can be found in the electronic version of Table 5. Atomic data include laboratory wavelengths, excitation potentials and log gf values, which are always taken from the VALD database, with the exceptions listed below.

3.1. α Elements Atomic Data

The only α-element for which we had clear problems with the atomic data was magnesium. The lines with χ_{ex}=5.75 eV (7060 and 7193Å) gave discrepant abundances by ∼1.5 dex with respect to the average of all Mg lines. We compared our VALD log gf with the NIST[12] database of atomic data and noticed a difference of 1.4 dex for the χ_{ex}=5.75 eV lines, while all the other Mg I had very similar log gf values in both databases. The NIST log gf values abundances of the χ_{ex}=5.75 eV lines gave abundances in much better agreement with the other Mg I lines and with the literature Mg abundances for OC, therefore we used the NIST values for those lines, instead of the VALD ones.

Another element with uncertain log gf values is Calcium. As an example, for the 9 lines we use, there is an average difference of $\log gf_{NIST}$–$\log gf_{VALD}$=–0.17±0.18 dex, which is not statistically significant given the large σ. Also, the NIST loggf values for those 9 lines all range from D to E, which means that they are largely uncertain. Finally, our solar abundance (Section 4.6) gives [Ca/H]=–0.09±0.03 (±0.03) dex if we use the VALD loggf and [Ca/H]=+0.08±0.03 (±0.03) dex with the NIST ones, which is equally compatible with zero within 3 sigma. Summarizing, there is large uncertainty on the Calcium loggf determinations, and we really should keep in mind that there is an additional ∼0.2 dex uncertainty on all [Ca/Fe] determinations in the literature.

For the synthesis of the [O I]–Ni I blend at 6300Å, we used the VALD log gf for oxygen, but we chose to use the Johansson et al. (2003) log gf for Ni I at 6300.35Å, which is lower (–2.11 dex instead of –1.74) and gives oxygen abundances more in line with the other α-elements.

3.2. Heavy Elements Atomic Data

For neodymium, we could only find three reliable lines, which apparently do not need any detailed HFS (hyper-fine splitting) analysis (Aoki et al., 2001), at 5092, 5249 and 5485 Å. However, the spread of their abundances was quite high (Table 7). The laboratory log gf published by Den Hartog et al. (2003) are very similar to the ones from VALD, except for the 5485 Å line, where they differ by 0.14 dex. Therefore, since the log gf values by Den Hartog et al. (2003) slightly reduced the spread in the [Nd/Fe], we used them instead of the VALD ones (see Table 5).

3.3. Equivalent Widths with DAOSPEC

The full description of how DAOSPEC works, including comparisons with the literature and several experiments with artificial and real spectra, can be found in Stetson & Pancino (2008). The instructions on how to install, configure and use

[9] http://www.eso.org/observing/dfo/quality/UVES/pipeline/solar_spectrum.html

[10] http://www.astro.uu.se/∼vald/

[11] ftp://ftp.noao.edu/fts/linelist/Moore

[12] http://physics.nist.gov/PhysRefData/ASD/index.html

Table 5. Equivalent Widths and Atomic Data of the programme stars. The complete version of the Table is available at the CDS. Here we show a few lines for guidance about its contents.

Cluster	Star	λ (Å)	Elem	χ_{ex} (eV)	$\log gf$ (dex)	EW (mÅ)	δEW (mÅ)	Q
Cr 110	2108	5055.99	Fe I	4.31	-2.01	41.2	3.3	0.371
Cr 110	2108	5178.80	Fe I	4.39	-1.84	45.4	7.1	0.851
Cr 110	2108	5294.55	Fe I	3.64	-2.86	–	–	–
Cr 110	2108	5285.13	Fe I	4.43	-1.64	50.1	5.2	0.607
Cr 110	2108	5295.31	Fe I	4.42	-1.69	38.3	9.5	1.958

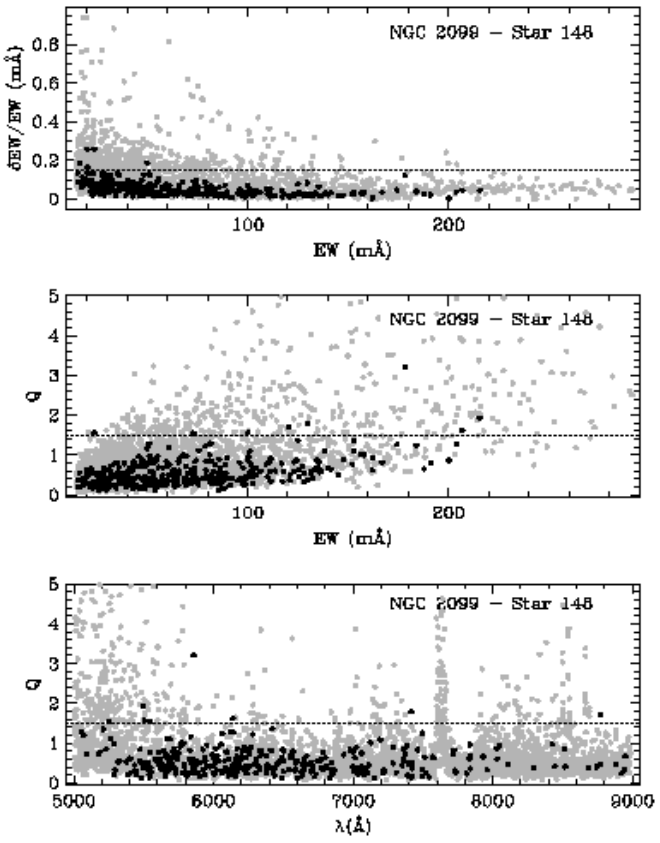

Fig. 2. The behaviour of DAOSPEC relative errors δEW/EW versus EW is shown (top panel) and the 15% error limit is marked with a dotted line. The behaviour of the quality parameter Q is shown versus EW (middle panel) and wavelength (bottom panel) and the Q=1.5 limit is marked with a dotted line. See Section 3.3 for more details. In all panels, grey dots represent all the lines measured by DAOSPEC, while black dots represent lines cross-identified with our input linelist.

DAOSPEC can be found in *"Cooking with DAOSPEC"*[13]. In short, DAOSPEC is a Fortran program that automatically finds absorption lines in a stellar spectrum, fits the continuum, measures EW, and identifies lines with a laboratory linelist; it also provides a radial velocity estimate (Section 2.2).

As described in Section 3, we used the DAOSPEC errors and quality parameter, Q, to select good absorption lines in our master line list. Since our spectra are rebinne linear in wavelength, we scaled the FWHM with λ. Figure 2 shows their behaviour. δEW is the formal error of the gaussian fit that DAOSPEC outputs, and $\delta EW/EW$ can be used to select good measurements, since smaller lines are noisier and tend to have higher relative errors. The quality parameter Q, instead, is the result of the comparison of local residuals around each line with average residuals on the whole spectrum. As a result Q tends to be worse for strong lines, because the Gaussian approximation does not hold so well anymore. Also, Q gets worse at the blue side of the spectrum, where the S/N ratio is lower. In the region around 7700 Å, where the residuals of the prominent O_2 telluric band disturb the measurements, Q reaches its maximum. The measured EW for our programme stars are shown in the electronic version of Table 5 along with the δEW and Q parameter estimated by DAOSPEC.

3.4. EW uncertainties

We used the formal errors of the Gaussian fit computed by DAOSPEC only to reject bad measurements from our initial line list. The actual abundance errors due to the EW measurements process itself were instead computed later, as explained in Section 4.3.

To compute the EW uncertainty due to the continuum placement, we used Equation 7 from Stetson & Pancino (2008) to derive the effective uncertainty on the continuum placement ($\pm\Delta C/C$), which turned out to be significantly smaller than 1%. We first lowered the "best" continuum by $\Delta C/C$ and measured EWs again, obtaining $EW_{(-)}$, then we increased it by the same amount and measured $EW_{(+)}$. The differences with the "correct" EW measurements, $\Delta EW_{(-)}$ and $\Delta EW_{(+)}$ were averaged to produce the actual ΔEW for each line. The typical resulting uncertainty, due only to the continuum placement, was approximately constant with EW and of ΔEW$\simeq$1 mÅ approximately (see also Figure 2 by Stetson & Pancino, 2008). Such a small uncertainty was neglected because it had a much smaller impact on the resulting abundances than other sources of uncertainty considered in Sections 4.3 and 4.4.

3.5. Comparison with Literature EW

To our knowledge, only one of our target stars was studied before by Yong et al. (2005) and Tautvaišiene (2000), with a resolution and S/N similar to ours, i.e. star 141 in M 67. While Yong et al. (2005) do not publish their EW measurements, we can compare with the ones by Tautvaišiene (2000). The authors provided two sets of EW, the former derived from a spectrum with R$\simeq$30000, and the latter from a spectrum with R$\simeq$60000. We have 48 lines in common with the R$\simeq$30000 set and 36 with the R$\simeq$60000 set.

Figure 3 shows good agreement between our EWs and the R$\simeq$30000 set. We found just a sistematic offset of EW_{T00}-

[13] http://www3.cadc-ccda.hia-iha.nrc-cnrc.gc.ca/community/STETSON/daospec/ ; http://www.bo.astro.it/~pancino/projects/daospec.html

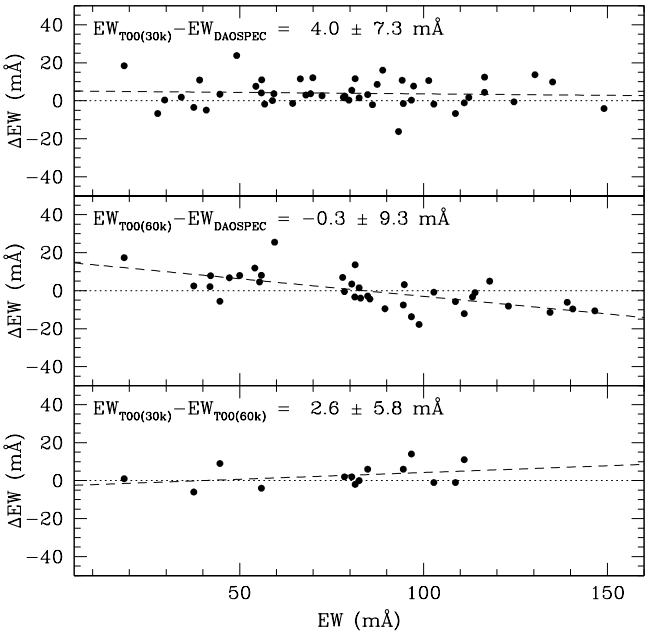

Fig. 3. Comparison of our EW measurements with Tautvaišiene (2000), for star 141 in M 67. The top panel shows the comparison of DAOSPEC EW with the R≃30000 set by Tautvaišiene (2000), based on 48 lines in common. The middle panel show the same comparison, but for the R≃60000 set by Tautvaišiene (2000), based on 36 lines. The bottom panel shows the 15 lines in common between the R≃30000 and the R≃60000 EW sets, considering only the lines included in the two upper panels.

$EW_{DAOSPEC}$ = 4.0 ± 7.3 mÅ, which corresponds to a continuum placement difference of about 1% (see also Section 3.4). A possible trend with EW was visible when comparing our EWs with the R≃60000 set, with no systematic offset ($\Delta EW = -0.3 \pm 9.3$ mÅ). On the one hand, this means that our continuum placement agrees much better with the R≃60000 continuum by Tautvaišiene (2000) than with the R≃30000 one. On the other hand, we noted that a possible trend is also visible when comparing the Tautvaišiene (2000) measurements at R≃30000 with those at R≃60000. In conclusion, we considered our EW measurements in good agreement with the Tautvaišiene (2000) ones, given the involved uncertainties (see also Table 6).

4. Abundance Analysis

4.1. Best Model Search

A preliminary abundance determination was done using the photometric parameters (Section 4), which allowed us to identify and remove those lines in our list that gave systematically discrepant abundances. We found largely discrepant Fe I and Fe II values when using the photometric parameters (by ≃0.5–0.9 dex), indicating that something was wrong with the photometric gravities (Section 2.3).

As a second step, we calculated Fe I and Fe II abundances for a set of models with parameters extending more than 3σ around the photometric estimates of Table 3, i.e., about ±300–500 K in $T_{\rm eff}$, ±0.3–0.6 dex in $\log g$ and ±0.5 km s^{-1} in v_t, depending on the star. This large grid of calculated abundances was used to refine our photometric estimate of the atmospheric parameters.

Table 6. Literature comparison for star 141 in M 67.

Parameter	Here	T00	Y05
Resolution	30000	30–60000	28000
S/N	70-100	≥100	30–100
T_eff (K)	4650	4730	4700
log$g$ (dex)	2.8	2.4	2.3
v_t (km s^{-1})	1.3	1.8	1.3
[FeI/H]	0.06±0.01(±0.10)	–0.01±0.02	–0.01±0.02
[FeII/H]	0.01±0.03(±0.10)	–0.01±0.05	0.01±0.03
[α/Fe]	0.01±0.01(±0.07)	0.01±0.03	0.12±0.06
[Al/Fe]	0.06±0.06(±0.05)	0.08±0.01	0.16±0.03
[Ba/Fe]	0.26±0.05(±0.06)	0.07±0.00	0.02±0.00
[Ca/Fe]	–0.13±0.02(±0.03)	0.09±0.05	0.09±0.02
[Co/Fe]	0.11±0.02(±0.06)	0.05±0.07	0.01±0.05
[Cr/Fe]	0.01±0.03(±0.06)	0.12±0.05	—
[La/Fe]	0.06±0.05(±0.09)	–0.06±0.00	0.13±0.03
[Mg/Fe]	0.29±0.03(±0.10)	0.11±0.00	0.18±0.02
[Na/Fe]	0.10±0.02(±0.04)	0.25±0.00	0.24±0.06
[Nd/Fe]	0.01±0.29(±0.10)	—	—
[Ni/Fe]	0.06±0.02(±0.03)	0.05±0.04	0.06±0.03
[O/Fe]	–0.05±0.09(±0.08)	0.04±0.00	0.10±0.04
[Sc/Fe]	–0.02±0.08(±0.08)	0.09±0.05	—
[Si/Fe]	0.09±0.02(±0.08)	0.11±0.04	0.11±0.04
[TiI/Fe]	–0.07±0.02(±0.07)	0.04±0.05	0.05±0.03
[TiII/Fe]	–0.07±0.08(±0.06)	0.11±0.07	—
[V/Fe]	0.13±0.04(±0.14)	0.09±0.03	—
[Y/Fe]	–0.04±0.02(±0.12)	–0.12±0.08	—

We chose the model that satisfied simultaneously (within the uncertainties[14]) the following conditions: *(i)* the abundance of Fe I lines should not vary with excitation potential χ_{ex}; *(ii)* the abundance of Fe I lines should not vary significantly with EW, i.e., strong and weak lines should give the same abundance[15]; *(iii)* the abundance of Fe I lines should not differ sigificantly from the abundance of Fe II lines; *(iv)* the abundance of Fe I lines should not vary significantly with wavelength.

Using the spreads of the Fe I and Fe II abundances of various lines, and the uncertainties in the slopes of the above conditions, we estimated the typical 1σ uncertainties on the spectroscopic parameters: about ±100 K on $T_{\rm eff}$, ±0.2 dex on $\log g$ and ±0.1 km s^{-1} on v_t.

The resulting spectroscopic parameters (Table 3) were always in good agreement with the photometric ones, within the quoted uncertainties, with a tendency of the spectroscopic gravities to be systematically higher by 0.3–0.5 dex (see above). However, these differences are always easily accomodated within the uncertainty ranges (due to photometric errors, uncertainties in distance moduli and reddenings, and bolometric corrections).

4.2. Abundance Calculations

Abundance calculations and spectral synthesis (for oxygen) were done using the last updated version of the abundance calculation code originally described by Spite (1967). We used the model atmospheres by Edvardsson et al. (1993). We also made

[14] We basically considered a slope consistent with zero when the 3 σ spread around the fit was larger than the maximum [Fe/H] difference implied by the fitted slope at the extremes of the interval covered by the abscissae (be it χ_{ex}, EW or λ).

[15] We decided not to use the Magain (1984) effect, because we prefer to have internally consistent abundances from each line, and the difference between the two methods in our case appears small ($\Delta v_t <$ 0.2 km s^{-1}).

use of ABOMAN, a tool developed by E. Rossetti at the INAF, Bologna Observatory, Italy, that allows for the semi-automatic processing of several objects, using the above abundance calculation codes. ABOMAN performs automatically all the steps needed to choose the best model, and provides all the graphical tools to analyze the results.

When the best model was found for each star, abundances and abundance ratios of all the species of interest were calculated, by averaging the results for each line of that element (Table 7). Abundance ratios were always computed with respect to Fe I. Cluster averages were computed as weighted averages of the results for each star in the cluster and, if necessary, of different ionization stages of each element (Table 8). In all Tables, [α/Fe] is the weighted average of all α-elements abundances.

We can compare our results for star 141 in M 67 (see also Section 3.5) with the ones by Tautvaišiene (2000) and Yong et al. (2005). We find a general agreement for both atmospheric parameter and abundance ratios, with the only significant exception of barium (but see the discussion in Section 6.3), calcium (discussed in Section 6.2) and titanium. For all the discussed elements our results, as discussed in Section 6, are in broad agreement with the whole body of high resolution abundances for OC, so we consider our results sound.

4.3. Internal Abundance Uncertainties

Random uncertainties in the EW measurement process and in the $\log gf$ determinations were taken into account by averaging the abundances determinations obtained for different lines and using $\sigma/\sqrt{(n_{lines})}$ as the final *internal* error. These are reported in Table 7, and they are of the order of ∼0.01 dex for Fe I which had the highest number of lines, and could reach up to ∼0.2–0.3 dex for elements relying on a handful of lines such as Nd, for example. Additional systematic (from line to line) and random (from star to star) uncertainties in EW measurements, due to continuum placement, had a negligible impact on the final abundances in our specific case (Section 3.4).

For the spectral synthesis of oxygen, the uncertainty of the fit was computed by bracketing the best fitting synthetic spectrum with two spectra with altered abundance. The bracketing spectra were chosen to overlap the 1σ poissonian uncertainty on the observed spectrum. The abundance difference of the two bracketing spectra with the best fit were averaged together to produce the estimated uncertainty, reported in Table 7 (and in our solar analysis, Table 10).

4.4. Uncertainties due to the Choice of Stellar Parameters

The choice of stellar parameters implies systematic (from line to line) and random (from star to star) uncertainties on the final abundances. Usually, to estimate the impact of the stellar parameter choice on the derived abundances, each parameter is altered by its estimated uncertainty and the resulting abundance differences with respect to the best model parameter abundance set are summed in quadrature to obtain a global uncertainty. We applied this method to our coolest (508 in NGC 2099) and warmest star (2129 in Cr 110) and obtained for the various abundance ratios uncertainties ranging from 0.05 to 0.45 dex, with a typical value around ∼0.10 dex.

However, as noted by Cayrel et al. (2004), this method produces a very conservative estimate of the uncertainty, because it neglects the natural correlation among stellar parameters occurring when the so called "spectroscopic method" (Section 4.1) is adopted. Covariance terms should therefore be included to properly take into account such dependencies among the parameters (see McWilliam et al., 1995, for a detailed treatment of the problem). The practical method proposed by Cayrel et al. (2004) assumes that T_{eff} largely dominates the abundance results and, therefore, T_{eff} has to be varied by its estimated uncertainty (≃100 K in our case, Section 4.1). A new "second best" model has to be identified with the new value of T_{eff} by varying v_t and $\log g$ accordingly, to minimize as much as possible the slopes of the relations described in Section 4.1. This method naturally and properly takes into account both the main terms of the error budget *and* the appropriate covariance terms.

We therefore altered the temperature of our hottest and coolest stars (see above) by +100 K and by –100 K. We re-optimized all the parameters and re-calculated all the abundance ratios. The final uncertainties are the average of the uncertainties calculated with the higher and lower temperature and are shown in Table 9. The average between the uncertainties of these two cases is taken as a reliable estimate for the impact of the choice of stellar parameters on our abundance ratios. We added these *external* uncertainties between parenthesis after each abundance ratio and we summed them in quadrature with the *internal* errors to produce the errobars in each Figure.

Table 9. Uncertanties due to the choice of stellar parameters.

Ratio	NGC2099-508 (T=4500 K)	Cr110-2129 (T=4950 K)	Average
[Al/Fe]	±0.04	±0.07	±0.05
[Ba/Fe]	±0.04	±0.08	±0.06
[Ca/Fe]	±0.03	±0.03	±0.03
[Co/Fe]	±0.07	±0.05	±0.06
[Cr/Fe]	±0.09	±0.03	±0.06
[Fe/H]	±0.16	±0.04	±0.10
[La/Fe]	±0.10	±0.07	±0.09
[Mg/Fe]	±0.11	±0.09	±0.10
[Na/Fe]	±0.03	±0.06	±0.04
[Nd/Fe]	±0.09	±0.12	±0.10
[Ni/Fe]	±0.02	±0.03	±0.03
[O/Fe]	±0.10	±0.07	±0.08
[Sc/Fe]	±0.07	±0.09	±0.08
[Si/Fe]	±0.12	±0.03	±0.07
[Ti/Fe]	±0.07	±0.06	±0.06
[V/Fe]	±0.21	±0.07	±0.14
[Y/Fe]	±0.15	±0.08	±0.12

4.5. Other Sources of Uncertainty

The following additional sources of systematic uncertainties are not explicitly discussed here, but should be taken into account when comparing our abundance estimates with other works in the literature:

- systematic uncertainties due to the choice of the solar reference abundances, which are not discussed here. Our abundances can be reported to any solar reference abundance with the information in Table 10;
- uncertainties due to the choice of $\log gf$ values, which can be estimated by comparing our $\log gf$ values with other literature values (see Section 3.1);
- uncertainties in the whole analysis due to more sophisticated effects such as, NLTE, HFS, isotope ratios, that are difficult to evaluate in some cases (these are mentioned whenever known or relevant in Sections 3 and 6;

Table 7. Abundance Ratios for sigle cluster stars, with their *internal* uncertainties (Section 4.3). For *external* uncertainties see Table 9

	Cr 110			NGC 2099 (M 37)			NGC 2420		
Ratio	Star 2108	Star 2129	Star 3144	Star 067	Star 148	Star 508	Star 041	Star 076	Star 174
[FeI/H]	0.02±0.01	0.05±0.01	0.02±0.01	0.01±0.01	–0.03±0.01	0.07±0.01	–0.07±0.01	–0.06±0.01	–0.03±0.01
[FeII/H]	0.00±0.06	–0.04±0.08	0.00±0.06	–0.01±0.02	–0.07±0.04	0.05±0.06	–0.09±0.06	0.00±0.02	–0.07±0.04
[α/Fe]	–0.02±0.02	0.01±0.02	0.04±0.02	–0.04±0.01	0.00±0.01	0.03±0.01	–0.03±0.01	–0.03±0.01	0.03±0.02
[Al/Fe]	–0.02±0.04	–0.06±0.08	–0.03±0.06	–0.06±0.08	–0.10±0.07	–0.04±0.07	–0.10±0.04	–0.10±0.05	–0.09±0.05
[Ba/Fe]	0.48±0.02	0.49±0.04	0.52±0.06	0.60±0.05	0.55±0.04	0.58±0.04	0.54±0.04	0.58±0.05	0.65±0.02
[Ca/Fe]	–0.08±0.04	–0.04±0.06	–0.09±0.07	–0.06±0.05	–0.08±0.04	–0.09±0.04	–0.08±0.03	–0.11±0.04	–0.08±0.05
[Co/Fe]	0.13±0.05	–0.08±0.04	0.01±0.04	–0.04±0.02	–0.04±0.02	–0.05±0.02	0.10±0.05	–0.02±0.03	0.05±0.03
[Cr/Fe]	0.00±0.04	0.06±0.06	0.03±0.08	–0.01±0.06	0.01±0.05	0.05±0.05	–0.02±0.03	–0.09±0.06	–0.02±0.05
[La/Fe]	0.11±0.09	0.12±0.03	–0.15±0.04	0.08±0.02	0.16±0.08	0.13±0.08	0.23±0.01	0.12±0.09	0.07±0.13
[Mg/Fe]	0.19±0.07	0.01±0.14	0.16±0.08	0.28±0.05	0.26±0.04	0.27±0.03	0.09±0.05	0.10±0.09	0.14±0.08
[Na/Fe]	–0.08±0.02	–0.06±0.08	0.00±0.03	0.08±0.05	0.10±0.04	0.05±0.08	–0.13±0.09	–0.04±0.06	0.02±0.07
[Nd/Fe]	0.05±0.16	0.29±0.13	0.51±0.28	0.23±0.29	0.26±0.25	0.33±0.32	0.12±0.16	0.40±0.28	0.18±N.A.
[Ni/Fe]	–0.02±0.02	–0.01±0.02	–0.04±0.03	–0.04±0.03	–0.02±0.02	–0.01±0.02	0.03±0.02	–0.01±0.02	–0.01±0.02
[O/Fe]	0.08±0.08	–0.07±0.12	0.02±0.14	0.12±0.07	0.25±0.15	0.22±0.13	–0.01±0.16	0.24±0.14	0.39±0.33
[Sc/Fe]	0.11±0.05	–0.07±0.06	–0.14±0.10	–0.05±0.05	–0.01±0.07	–0.02±0.12	0.07±0.01	0.11±0.07	0.16±0.06
[Si/Fe]	0.02±0.03	0.04±0.02	0.06±0.03	0.07±0.03	0.11±0.02	0.06±0.03	0.05±0.02	0.05±0.02	0.02±0.03
[TiI/Fe]	0.01±0.03	0.00±0.03	0.01±0.04	–0.10±0.02	–0.10±0.02	–0.07±0.02	–0.06±0.02	–0.09±0.02	0.06±0.03
[TiII/Fe]	0.01±0.13	–0.04±0.07	0.11±0.05	–0.01±0.06	0.00±0.05	0.05±0.08	–0.04±0.23	0.07±0.09	0.12±0.07
[V/Fe]	0.28±0.06	–0.03±0.05	–0.09±0.07	–0.09±0.02	–0.08±0.04	–0.03±0.04	0.11±0.06	–0.08±0.05	0.13±0.04
[Y/Fe]	0.02±0.12	–0.17±0.08	–0.03±0.18	–0.03±0.23	0.09±0.09	0.08±0.20	–0.14±0.14	0.06±0.02	0.02±0.09

	NGC 2682 (M 67)			NGC 7789		
Ratio	Star 141	Star 223	Star 286	Star 5237	Star 7840	Star 8556
[FeI/H]	0.06±0.01	0.04±0.01	0.06±0.01	–0.01±0.01	0.03±0.01	0.12±0.01
[FeII/H]	0.01±0.03	0.02±0.05	–0.05±0.04	–0.06±0.05	–0.03±0.07	0.07±0.06
[α/Fe]	0.01±0.01	–0.03±0.01	–0.05±0.01	–0.02±0.02	–0.02±0.02	–0.08±0.02
[Al/Fe]	0.06±0.06	0.02±0.05	0.03±0.05	–0.01±0.10	0.05±0.11	–0.13±0.10
[Ba/Fe]	0.26±0.05	0.27±0.05	0.23±0.05	0.49±0.06	0.36±0.07	0.46±0.03
[Ca/Fe]	–0.13±0.02	–0.20±0.03	–0.15±0.02	–0.10±0.04	–0.12±0.07	–0.24±0.03
[Co/Fe]	0.11±0.02	0.05±0.04	0.17±0.04	–0.02±0.04	–0.03±0.02	–0.01±0.03
[Cr/Fe]	0.01±0.03	–0.01±0.04	0.06±0.05	0.05±0.04	–0.02±0.03	0.16±0.45
[La/Fe]	0.06±0.05	–0.06±0.06	0.07±0.03	0.14±0.06	0.06±0.07	0.14±0.15
[Mg/Fe]	0.29±0.03	0.20±0.08	0.23±0.05	0.26±0.07	0.24±0.04	0.13±0.06
[Na/Fe]	0.10±0.02	–0.02±0.04	0.22±0.08	0.04±0.01	0.09±0.08	–0.15±0.01
[Nd/Fe]	0.01±0.29	0.10±0.25	0.10±0.21	0.21±0.38	–0.17±0.27	0.35±0.20
[Ni/Fe]	0.06±0.02	0.04±0.02	0.04±0.02	–0.02±0.02	0.00±0.02	–0.02±0.03
[O/Fe]	–0.05±0.09	0.09±0.11	0.13±0.10	0.21±0.15	0.13±0.10	0.23±0.20
[Sc/Fe]	–0.02±0.08	–0.05±0.04	0.01±0.05	0.10±0.09	0.06±0.10	0.08±0.12
[Si/Fe]	0.09±0.02	0.12±0.02	0.06±0.02	–0.01±0.02	–0.02±0.03	0.03±0.04
[TiI/Fe]	–0.07±0.02	–0.11±0.02	0.00±0.02	–0.02±0.03	–0.03±0.03	–0.14±0.04
[TiII/Fe]	–0.07±0.08	0.02±0.06	–0.06±0.13	–0.07±0.29	–0.19±0.17	0.14±0.05
[V/Fe]	0.13±0.04	0.06±0.04	0.25±0.04	0.05±0.04	–0.01±0.04	–0.16±0.06
[Y/Fe]	–0.04±0.02	–0.06±0.05	0.00±0.03	0.22±N.A.	–0.01±N.A.	0.07±0.18

– small additional uncertainties due to the particular choice of atmospheric models and of the abundance calculation code.

4.6. The Sun

To test the whole abundance determination procedure, including EW measurement, choice of lines and atomic parameters, and the uncertainties determination criteria, we performed an abundance analysis of the Sun, and checked that we obtain solar values for all elements, within the uncertainties. We used the solar spectrum from the ESO spectrograph HARPS, in La Silla, Chile, obtained by observing Ganymede[16]. The spectral resolution, R≃45000, is comparable to ours, while the S/N≃350 is much higher.

To measure EWs, we used DAOSPEC and the same linelist used for our programme stars. We then compared our solar EWs with two different literature sets, the first by Moore et al. (1966) and the second by Rutten & van der Zalm (1984). The median difference between our EW and the ones by Moore is EW_{DAO}–EW_{Moore}=0.9 mÅ (with an inter-quartile range of ±2.7 mÅ), based on 225 lines in common, while the one with the Rutten & van der Zalm (1984) measurements is EW_{DAO}–EW_{RZ84}=–0.5 mÅ (with an inter-quartile range of ±2.1 mÅ), based on 112 lines in common. For completeness, we note that EW_{Moore}–EW_{RZ84}=1.5 mÅ (with an inter-quartile range of ±2.8 mÅ), based on 390 lines in common. We are therefore satisfied with our solar EW measurements.

We then performed our abundance analysis (as in Section 4.2) by exploring the following atmospheric parameters ranges: $T_{\rm eff,\odot}$=5700–5800, in steps of 50 K; $\log g_\odot$=4.3–4.5, in steps of 0.1 dex; and v_t=0.5–1.5, in steps of 0.1 km s^{-1}. The resulting best model has $T_{\rm eff,\odot}$=5750 K; $\log g_\odot$=4.4 dex; and v_t=0.8 km s^{-1}, in good agreement with the accepted values (Andersen, 1999). Our adopted reference solar abundances

[16] http://www.ls.eso.org/lasilla/sciops/3p6/harps/monitoring/sun.html

Table 8. Average cluster abundances, obtained with the weighted average of the single stars abundances.

Ratio	Cr 110	NGC 2099	NGC 2420	M 67	NGC 7789
[Fe/H]	+0.03±0.02(±0.10)	+0.01±0.05(±0.10)	–0.05±0.03(±0.10)	+0.05±0.02(±0.10)	+0.04±0.07(±0.10)
[α/Fe]	+0.01±0.03(±0.07)	0.00±0.04(±0.07)	–0.02±0.03(±0.07)	–0.02±0.03(±0.07)	–0.04±0.03(±0.07)
[Al/Fe]	–0.04±0.02(±0.05)	–0.06±0.03(±0.05)	–0.10±0.01(±0.05)	+0.03±0.02(±0.05)	–0.03±0.09(±0.05)
[Ba/Fe]	+0.49±0.02(±0.06)	+0.57±0.02(±0.06)	+0.62±0.07(±0.06)	+0.25±0.02(±0.06)	+0.45±0.05(±0.06)
[Ca/Fe]	–0.07±0.02(±0.03)	–0.08±0.01(±0.03)	–0.09±0.02(±0.03)	–0.16±0.03(±0.03)	–0.18±0.09(±0.03)
[Co/Fe]	+0.01±0.10(±0.06)	–0.04±0.01(±0.06)	+0.03±0.06(±0.06)	+0.08±0.06(±0.06)	–0.02±0.01(±0.06)
[Cr/Fe]	+0.02±0.03(±0.06)	+0.02±0.03(±0.06)	–0.03±0.03(±0.06)	+0.01±0.03(±0.06)	+0.01±0.05(±0.06)
[La/Fe]	+0.03±0.18(±0.09)	+0.09±0.05(±0.09)	+0.23±0.09(±0.09)	+0.05±0.06(±0.09)	+0.11±0.05(±0.09)
[Mg/Fe]	+0.16±0.07(±0.10)	+0.27±0.01(±0.10)	+0.09±0.06(±0.10)	+0.27±0.04(±0.10)	+0.22±0.07(±0.10)
[Na/Fe]	–0.06±0.05(±0.04)	+0.09±0.02(±0.04)	–0.04±0.07(±0.04)	+0.08±0.09(±0.04)	–0.05±0.13(±0.04)
[Nd/Fe]	+0.23±0.20(±0.10)	+0.27±0.05(±0.10)	+0.19±0.17(±0.10)	+0.08±0.05(±0.10)	+0.17±0.30(±0.10)
[Ni/Fe]	–0.02±0.01(±0.03)	–0.02±0.01(±0.03)	+0.00±0.02(±0.03)	+0.05±0.01(±0.03)	–0.01±0.01(±0.03)
[O/Fe]	+0.03±0.08(±0.08)	+0.15±0.08(±0.08)	+0.15±0.18(±0.08)	+0.04±0.10(±0.08)	+0.16±0.06(±0.08)
[Sc/Fe]	+0.01±0.13(±0.08)	–0.03±0.03(±0.08)	+0.07±0.05(±0.08)	–0.03±0.04(±0.08)	+0.08±0.02(±0.08)
[Si/Fe]	+0.04±0.02(±0.07)	+0.09±0.03(±0.07)	+0.04±0.01(±0.07)	+0.10±0.02(±0.07)	–0.01±0.02(±0.07)
[Ti/Fe]	+0.02±0.04(±0.06)	–0.08±0.04(±0.06)	–0.04±0.08(±0.06)	–0.04±0.06(±0.06)	–0.03±0.09(±0.06)
[V/Fe]	+0.05±0.19(±0.14)	–0.08±0.03(±0.14)	–0.05±0.13(±0.14)	+0.15±0.13(±0.14)	–0.01±0.09(±0.14)
[Y/Fe]	–0.10±0.12(±0.12)	+0.07±0.06(±0.12)	+0.05±0.08(±0.12)	–0.05±0.04(±0.12)	+0.08±0.09(±0.12)

Table 10. Solar abundance values.

Element	$[X/H]_{derived}$	$\log\epsilon_{GS96}$	$\log\epsilon_{A05}$
Al	–0.34±N.A.(±0.05)	6.47±0.07	6.37±0.07
Ba	+0.34±0.02(±0.06)	2.13±0.05	2.17±0.07
Ca	–0.09±0.03(±0.03)	6.36±0.02	6.31±0.04
Co	+0.05±0.02(±0.06)	4.92±0.04	4.92±0.08
Cr	+0.02±0.05(±0.06)	5.67±0.03	5.64±0.10
FeI	+0.01±0.01(±0.10)	7.50±0.04	7.45±0.05
FeII	–0.03±0.02(±0.10)	7.50±0.04	7.45±0.05
La	—	1.17±0.07	1.13±0.05
Mg	—	7.58±0.05	7.53±0.09
Na	–0.10±0.01(±0.04)	6.33±0.03	6.17±0.04
Nd	—	1.42±0.06	1.45±0.05
Ni	+0.01±0.01(±0.03)	6.25±0.01	6.23±0.04
O	-0.01±0.07(±0.08)	8.87±0.07	8.66±0.05
Sc	+0.06±0.02(±0.08)	3.17±0.10	3.05±0.08
Si	–0.08±0.01(±0.07)	7.55±0.05	7.51±0.04
Ti	+0.03±0.05(±0.06)	5.02±0.06	4.90±0.06
V	–0.14±0.02(±0.14)	4.00±0.02	4.00±0.02
Y	—	2.24±0.03	2.21±0.02

(Grevesse et al., 1996) are shown in Table 10, along with the abundance ratios derived as described. As can be seen, all the derived abundance ratios are compatible with zero, within the uncertainties, with the exception of Al and Ba. For Al, only one (λ=6698Å) very weak (EW=18 mÅ) line could be measured in the solar spectrum, while we used about 8 lines for the analysis of our red clump giants. The lines at 6696 amd 6698Å are known to give tendentially lower values than the other Al lines (Reddy et al., 2003; Gratton et al., 2001), so we do not worry too much that our lone 6698Å[17] solar line gives a low [Al/Fe] result. Ba is discussed in Section 6.3. For some elements (La, Mg, Nd, Y) no ratio could be determined either because their lines appear too weak in the sun, or because the solar spectrum range (5000–7000Å) does not contain the lines we used in this paper.

[17] Due to the shorter spectral range of the solar spectrum and to a spectral defect, we could only measure one Al line in the Sun.

5. Cluster-by-Cluster Discussion

5.1. Cr 110

Collinder 110 is a poorly studied, intermediate-age OC located at α_{J2000}=06:38:24 and δ_{J2000}=+02:01:00. We could not find any high resolution spectroscopic study of this cluster in the literature, but photometric studies have been conducted by Tsarevskii & Abakumov (1971), Dawson & Ianna (1998) and Bragaglia & Tosi (2003). Reddening, distance and ages determined by these authors are included in Table 4. Concerning metallicity, while the first two studies assume solar metallicity, Bragaglia & Tosi (2003) find, as a result of their synthetic diagram analysis, two equally good solutions, one at solar metallicity and the other at slightly sub-solar metallicity (Z=0.008). A re-evaluation of the same data by Bragaglia & Tosi (2006) favours the slightly subsolar value.

Low resolution spectroscopy using the infrared calcium triplet by Carrera et al. (2007) gave: [Fe/H]=–0.01±0.07 dex in the Carretta & Gratton (1997) scale, [Fe/H]=0.0±0.3 dex in the Zinn & West (1984) scale and [Fe/H]=–0.19±0.21 dex in the Kraft & Ivans (2003) scale. Our determination of [Fe/H]=+0.03±0.02 (±0.10) dex is in good agreement with all these estimates, given the large uncertainties involved in photometric and low-resolution spectroscopic metallicity estimates. The other element ratios determined here have no previous literature values to compare with, but the comparisons in Section 6 show that they behave like expected for a solar metallicity OC. Our radial velocity estimate for Cr 110, $<V_r>$=41.0±3.8 km s^{-1} (Section 2.2), is in good agreement with the CaT value by Carrera et al. (2007) of 45±8 km s^{-1}.

5.2. NGC 2099 (M 37)

NGC 2099 (M 37) is located in the Galactic anti-center direction in Auriga α_{J2000}=05:52:18 and δ_{J2000}=+32:33:12. Since it is near and it appears as a relatively rich and large cluster, it has been photometrically studied by several authors to derive accurate magnitudes, proper motions, and a census of variable stars (for historical references see Kalirai et al., 2001). All the papers that derived reddening, distance and age are also cited in Table 4. Photometric studies generally attribute a solar metal-

Table 11. Literature abundance determinations for M 67 based on high resolution spectroscopy.

	Here	T00[a]	S00[b]	Y05[c]	R06[d]	P08[e]	S09[f]
R=$\lambda/\delta\lambda$	30000	30–60000	30000	28000	45000	100000	50000
S/N	50–100	≥100	40–70	30–100	90–180	≃80	100–300
[Fe/H]	+0.05±0.02(±0.10)	–0.03±0.04	–0.05±0.01	+0.02±0.01	+0.03±0.01	+0.03±0.04	0.00±0.01
[Al/Fe]	+0.03±0.02(±0.05)	+0.14±0.07	—	+0.17±0.01	–0.06±0.04	–0.03±0.11	—
[Ba/Fe]	+0.25±0.02(±0.06)	+0.07±0.12	+0.21±0.20	–0.02±0.03	—	—	—
[Ca/Fe]	–0.16±0.03(±0.03)	+0.05±0.09	–0.02±0.03	+0.07±0.02	+0.05±0.04	+0.03±0.07	—
[Co/Fe]	+0.08±0.06(±0.06)	+0.08±0.07	—	—	—	—	—
[Cr/Fe]	+0.01±0.03(±0.06)	+0.10±0.09	—	—	–0.01±0.04	+0.03±0.09	—
[La/Fe]	+0.05±0.06(±0.09)	+0.13±0.10	—	+0.11±0.02	—	—	—
[Mg/Fe]	+0.27±0.04(±0.10)	+0.10±0.06	–0.11±0.08	+0.16±0.02	–0.01±0.03	—	—
[Na/Fe]	+0.08±0.09(±0.04)	+0.19±0.08	–0.05±0.05	+0.30±0.03	+0.04±0.07	–0.02±0.07	—
[Ni/Fe]	+0.05±0.01(±0.10)	+0.04±0.08	+0.04±0.06	+0.08±0.02	–0.01±0.04	–0.02±0.07	—
[O/Fe]	+0.04±0.10(±0.03)	+0.02±0.06	–0.02±0.08	+0.07±0.02	–0.04±0.01	–0.07±0.09	—
[Sc/Fe]	–0.03±0.04(±0.08)	+0.10±0.06	—	—	—	—	—
[Si/Fe]	+0.10±0.02(±0.07)	+0.10±0.05	—	+0.09±0.03	+0.03±0.04	–0.03±0.06	—
[Ti/Fe]	–0.04±0.06(±0.06)	+0.04±0.13	—	+0.12±0.02	–0.03±0.04	–0.02±0.11	—
[V/Fe]	+0.15±0.13(±0.14)	+0.15±0.16	—	—	—	—	—
[Y/Fe]	–0.05±0.04(±0.12)	+0.01±0.14	—	—	—	—	—

[a] Tautvaišiene (2000), from 6 red clump stars.
[b] Shetrone & Sandquist (2000), from 4 turn-off stars (we ignored blue stragglers).
[c] Yong et al. (2005), from 3 red clump stars.
[d] Randich et al. (2006), from 8 dwarfs and 2 slightly evolved stars.
[e] Pace et al. (2008), from 6 main sequence stars.
[f] Santos et al. (2009), from 3 red clump giants and 6 dwarfs.

licity to NGC 2099 (e.g., Mermilliod et al., 1996). Metallicity estimates based on photometry can only be found in Janes et al. (1988), who give [Fe/H]=0.09 dex; Marshall et al. (2005), who give [M/H]=+0.05 ±0.05 and Kalirai & Tosi (2004), who give Z<0.02.

Surprisingly, when considering the wealth of photometric studies, M 37 lacks any specific low or high resolution study aimed at determining its chemical composition. Our values therefore fill this gap, and show that in all respects this cluster has a typical solar metallicity, with all element ratios close to zero within the uncertainties. On the other hand, radial velocity determinations for this cluster are quite abundant (Section 2.2) and appear in good agreement with our determination.

5.3. NGC 2420

NGC 2420 (α_{J2000}=07:38:23 and δ_{J2000}=+21:34:24) has always been considered the definitive example of the older, moderately metal-deficient OC beyond the solar circle. Several good quality imaging studies appeared already in the 60s and 70s (Sarma & Walker, 1962; West, 1967b; Cannon & Lloyd, 1970; van Altena & Jones, 1970; McClure et al., 1974, 1978, to name a few), and more recent photometries appeared in a variety of photometric systems (the most cited being Anthony-Twarog et al., 1990). Its intermediate status between the solar-metallicity OC near the sun and the clearly metal-deficient population of globular clusters tagged it early on as a potential transition object between the two populations, with metallicity determinations — both photometric and spectroscopic — placing it at an [Fe/H] value around the one of 47 Tuc (e.g. Pilachowski et al., 1980; Cohen, 1980; Canterna et al., 1986; Smith & Suntzeff, 1987). More recent photometric works give somewhat higher [Fe/H] values, ranging from –0.5 to –0.3 dex (e.g. Twarog et al., 1997; Friel et al., 2002; Anthony-Twarog et al., 2006), but still significantly lower than the value of [Fe/H]=–0.05±0.03 (±0.10) dex we found here.

However, both Cohen (1980) and Pilachowski et al. (1980) noted that NGC 2420 should be significantly more metal rich than the Globular Clusters they analyzed, i.e., M 71 (Cohen, 1980) and 47 Tuc (Pilachowski et al., 1980), by some ≃0.5 dex. Since they placed M 71 and 47 Tuc around [Fe/H]=–1.3, they consequently placed NGC 2420 at [Fe/H]=–0.6. The resolution of their spectra (R<10000) was much lower than ours, but if we trust their analysis in a relative sense, and consider more recent metallicity estimates for 47 Tuc and M 71 (–0.76 and –0.73 respectively, Harris, 1996), we would then place NGC 2420 around [Fe/H]≃–0.1 or –0.2. Having said that, it is surprising that there are no modern high resolution studies of a cluster that was considered so important in the past. The highest spectral resolution employed to study NGC 2420 is R≃15000 (Smith & Suntzeff, 1987), with a spectral coverage of only 200Å, giving [Fe/H]=–0.57. Only the preliminary work of Freeland et al. (2002) has suggested a higher, slightly subsolar [Fe/H] value for NGC 2420. We also note that our [Fe/H] brings NGC 2420 more in line with other OC in the Galactic trends discussed in Section 7. Also, we cannot ignore the similarity with the case of NGC 7789 (Section 5.5), where high resolution spectroscopy by Tautvaišienė et al. (2005) and us provides a much higher abundance than the previous photometric and low/medium-resolution studies. Clearly, further high resolution spectroscopy with modern instruments, possibly with R≃50000 and S/N≃100 is needed for this cluster.

5.4. NGC 2682 (M 67)

Among the old OC, M 67 (α_{J2000}=08:51:18, δ_{J2000}=+11:48:00) is quite close to us, with low reddening (Table 4) and solar metallicity, so it is one of the most studied open clusters, and a good target to look for solar twins and analogs (Pasquini et al.,

Table 12. Literature abundance determinations for NGC 7789 based on high resolution spectroscopy.

	Here	T05[a]
R=$\lambda/\delta\lambda$	30000	30000
S/N	50–100	$\geq$ 50
[Fe/H]	+0.04±0.07(±0.10)	–0.04±0.05
[Al/Fe]	–0.03±0.09(±0.05)	+0.18±0.08
[Ca/Fe]	–0.18±0.09(±0.03)	+0.14±0.07
[Co/Fe]	–0.02±0.01(±0.06)	+0.09±0.14
[Cr/Fe]	+0.01±0.05(±0.06)	–0.05±0.09
[Mg/Fe]	+0.22±0.07(±0.10)	+0.18±0.07
[Na/Fe]	–0.05±0.13(±0.04)	+0.28±0.07
[Ni/Fe]	–0.01±0.01(±0.10)	–0.02±0.05
[O/Fe]	+0.16±0.06(±0.03)	–0.07±0.09
[Sc/Fe]	+0.08±0.02(±0.08)	–0.02±0.07
[Si/Fe]	–0.01±0.02(±0.07)	+0.14±0.05
[Ti/Fe]	–0.03±0.09(±0.06)	–0.03±0.07
[V/Fe]	–0.01±0.09(±0.14)	+0.09±0.12
[Y/Fe]	+0.08±0.09(±0.12)	+0.13±0.13

[a] Tautvaišienė et al. (2005), from 6 giants and 3 red clump giants.

2008). Since the first pioneering studies at the beginning of XX century, we have a few hundred papers published to date (see Burstein et al., 1986; Carraro et al., 1996; Yadav et al., 2008, for more references). Therefore, we have included M 67 in our sample because it acts as a fundamental comparison object, that enables us to place our measurements in a more general framework.

Among the vast literature on M 67, there are several determinations of its metallicity, with various methods (e.g. Demarque, 1980; Cohen, 1980; Foy & Proust, 1981; Janes & Smith, 1984; Burstein et al., 1984, 1986; Brown, 1987; Garcia Lopez et al., 1988; Cayrel de Strobel, 1990; Hobbs & Thorburn, 1991; Friel & Boesgaard, 1992; Friel & Janes, 1993; Janes & Phelps, 1994; Friel et al., 2002; Balaguer-Núñez et al., 2007; Marshall et al., 2005, to name a few), all typically converging to a solar value. high resolution abundance determinations have been derived for both giants and dwarfs, with many studies devoted to light elements such as lithium and beryllium and their implications for mixing theories (Pasquini et al., 1997; Jones et al., 1999; Randich et al., 2007).

Table 11 shows a comparison of our results with some of the most recent high resolution (R≥20000) determinations (Tautvaišiene, 2000; Shetrone & Sandquist, 2000; Randich et al., 2006; Pace et al., 2008; Santos et al., 2009). The overall comparison is extremely satisfactory for all elements, except maybe for Mg, Na, Ba and Ca (see also Section 3.1). For Mg, Na and Ba the large spread in literature demonstrates the difficulties in measuring these elements. For Ca we see that our value is marginally lower than other literature deterrminations. As explained in Section 3.1, this is most probably due to the large uncertainties on the Calcium log gf values.

5.5. NGC 7789

NGC7789 (α_{J2000}=23:57:24 and δ_{J2000}=+56:42:30, or l=115.53 and b=–5.39) is a rich and intermediate-age OC, with a well defined giant branch, a well-populated main-sequence turnoff, and a substantial population of blue stragglers (McNamara, 1980; Twarog & Tyson, 1985; Milone & Latham, 1994). Several photometric studies have been carried out (some examples are Kustner, 1923; Reddish, 1954; Burbidge & Sandage, 1958; Janes, 1977; Martinez Roger et al., 1994; Jahn et al., 1995; Gim et al., 1998a; Vallenari et al., 2000; Bartašiutė & Tautvaišienė, 2004; Bramich et al., 2005) and its parameters are reasonably well known.

Abundance determinations through photometry and low/medium-resolution spectroscopy all give sub-solar values around [Fe/H]≃–0.2 (Pilachowski, 1985; Friel & Janes, 1993; Schönberner et al., 2001; Friel et al., 2002), i.e., much lower than our [Fe/H]=0.04±0.07 (±0.10) dex. However, a more conforting comparison with Tautvaišienė et al. (2005) is shown in Table 12. Their spectra have resolution and S/N similar to ours, and most abundance ratios in common show an excellent agreement. Minor discrepancies arise for some elements such as Ca (but see the discussions in Sections 3.1 and 5.4), Al (but they used only one doublet while we used four), Na and O. Since they do not list their log gf values, and other ingredients of the abundance analysis were similar to ours, we cannot explain the Na-O discrepancies, but we suspect that they must be due log gf differences.

6. Abundance Ratios Discussion

We compare our abundance ratios with data from the literature, assembled as follows. For the Milky Way field stars, we use the Thick and Thin Disc measurements from Reddy et al. (2003) and Reddy et al. (2006), who performed homeogeneous abundance calculations of a few hundred F/G dwarfs selected from the Hipparcos catalogue. We added abundance ratios, based on high resolution spectroscopy, for 57 old OC from various literature sources (Table 13). When more than one determination was available for one cluster, we simply plotted them all to give a realistic idea of the uncertainties involved in the compilation.

6.1. Iron-peak Elements Ratios

When compared with literature (Figure 4), our iron-peak elements appear all solar and in good agreement with the results for the Disc and other OC. In particular, cobalt and chromium have the best agreement and smallest spreads. Although Sc, V and Co are known to possess HFS that may lead to an increased scatter and an overestimated ratio, they do not appear significantly different from solar for our target stars, so we did not attempt any detailed HFS analysis. Nevertheless, the effect of increased scatter and overestimated abundance are visible, expecially for vanadium, both in our data and in the Discs stars, as well as in the other clusters from the literature.

A puzzling effect is seen in Figure 4 in the [Ni/Fe] ratio. All the data from Disc stars are very close to solar (<[Ni/Fe]>=–0.02±0.02), and so are our determinations (<[Ni/Fe]>=0.00±0.03), but the other OC high resolution data appear slightly enhanced (<[Ni/Fe]>=0.06±0.04), lying systematically above the Disc ones. Such a ≃0.05 dex offset is well within the uncertainties of abundance determinations in general, but since it appears systematic in nature, we are still left without a clear explanation. Our [Ni/Fe] ratios anyway are a bit lower than the other OC determinations, although still compatible within the uncertainties.

6.2. α-elements Ratios

We obtained abundances of Ca, Mg, O, Si and Ti. As can be seen from Figure 5, Si and Ti appear practically solar, within the respective uncertainties, and in very good agreement with litera-

Table 13. Literature sources and [Fe/H] values for high resolution (R≥15000) based abundance ratios of old OC.

Cluster	[Fe/H]	Reference	Cluster	[Fe/H]	Reference
Be 17	–0.10	Friel et al. (2005)	NGC 2141	–0.26	Yong et al. (2005)
Be 20	–0.61	Yong et al. (2005)		0.00	Jacobson et al. (2009)
	–0.30	Sestito et al. (2008)	NGC 2158	–0.03	Jacobson et al. (2009)
Be 22	–0.32	Villanova et al. (2005)	NGC 2243	–0.48	Gratton & Contarini (1994)
Be 25	–0.20	Carraro et al. (2007)	NGC 2324	–0.17	Bragaglia et al. (2008)
Be 29	–0.44	Carraro et al. (2004)	NGC 2360	+0.07	Hamdani et al. (2000)
	–0.18	Yong et al. (2005)		+0.04	Smiljanic et al. (2008)
	–0.31	Sestito et al. (2008)	NGC 2420	–0.57	Smith & Suntzeff (1987)
Be 31	–0.40	Yong et al. (2005)	NGC 2447	+0.03	Hamdani et al. (2000)
Be 32	–0.29	Bragaglia et al. (2008)	NGC 2477	+0.07	Bragaglia et al. (2008)
Be 66	–0.48	Villanova et al. (2005)		–0.01	Smiljanic et al. (2008)
Be73	–0.22	Carraro et al. (2007)	NGC 2506	–0.20	Carretta et al. (2004)
Be75	–0.22	Carraro et al. (2007)	NGC 2660	+0.04	Bragaglia et al. (2008)
Blanco 1	+0.04	Ford et al. (2005)	NGC 3532	+0.04	Smiljanic et al. (2008)
Cr 261	–0.22	Friel et al. (2003)	NGC 3680	–0.04	Pace et al. (2008)
	–0.03	Carretta et al. (2005)		+0.04	Smiljanic et al. (2008)
	–0.03	De Silva et al. (2007)	NGC 3960	+0.02	Bragaglia et al. (2008)
	+0.13	Sestito et al. (2008)	NGC 5822	+0.04	Smiljanic et al. (2008)
Hyades	+0.13	Sestito et al. (2003)	NGC 6134	+0.15	Carretta et al. (2004)
	+0.13	Paulson et al. (2003)		+0.12	Smiljanic et al. (2008)
	+0.13	De Silva et al. (2006)	NGC 6253	+0.46	Carretta et al. (2007)
IC 2391	–0.03	Randich et al. (2001)		+0.36	Sestito et al. (2007)
IC 2602	–0.05	Randich et al. (2001)	NGC 6281	+0.05	Smiljanic et al. (2008)
IC 2714	+0.12	Smiljanic et al. (2008)	NGC 6475	+0.14	Sestito et al. (2003)
IC 4756	–0.15	Jacobson et al. (2007)	NGC 6633	+0.07	Smiljanic et al. (2008)
	+0.04	Smiljanic et al. (2008)	NGC 6791	+0.40	Peterson & Green (1998)
IC 4651	+0.11	Carretta et al. (2004)		+0.35	Origlia et al. (2006)
	+0.10	Pasquini et al. (2004)		+0.39	Carraro et al. (2006)
	+0.12	Pace et al. (2008)		+0.47	Carretta et al. (2007)
M 11	+0.10	Gonzalez & Wallerstein (2000)		+0.30	Boesgaard et al. (2009)
M 34	+0.07	Schuler et al. (2003)	NGC 6819	+0.09	Bragaglia et al. (2001)
M 67	–0.03	Tautvaišiene (2000)	NGC 6939	0.00	Jacobson et al. (2007)
	–0.01	Yong et al. (2005)	NGC 7142	+0.08	Jacobson et al. (2008)
	+0.03	Randich et al. (2006)	NGC 7789	–0.04	Tautvaišienė et al. (2005)
	+0.03	Pace et al. (2008)	Pleiades	–0.03	Randich et al. (2001)
Mel 66	–0.38	Gratton & Contarini (1994)		+0.06	Gebran & Monier (2008)
	–0.33	Sestito et al. (2008)	Praesepe	+0.04	Friel & Boesgaard (1992)
Mel 71	–0.30	Brown et al. (1996)		+0.12	Pace et al. (2008)
NGC 188	+0.01	Randich et al. (2003)	Rup 4	–0.09	Carraro et al. (2007)
NGC 1817	–0.07	Jacobson et al. (2009)	Rup 7	–0.26	Carraro et al. (2007)
NGC 1883	–0.20	Villanova et al. (2007)	Saurer 1	–0.38	Carraro et al. (2004)
	–0.01	Jacobson et al. (2009)	Tom 2	–0.45	Brown et al. (1996)
NGC 2112	–0.10	Brown et al. (1996)		–0.28	Frinchaboy et al. (2008)

ture determinations for both the Discs stars and the other OC. O, Ca and Mg give instead marginally discrepant enhancements.

For O, we note that the spread both in our data and in the literature is greater that in any other α-element. This is partly due to the well known problems of determining O from the 6300Å lone line, or the 6363Å weak line, or from the IR triplet at 7770Å, that requires NLTE corrections. Moreover, some old literature work uses Solar reference abundances reaching as high as 8.93, which can explain some of the lowest [O/Fe] literature estimates. Given the large spread, the tendency of our [O/Fe] measurements to lie on the upper envelope of the other OC high resolution data is probably irrelevant. Solar O enhancements would probably be more in line with the other α-elements, while the sub-solar values found generally in literature point towards Wolf-Rayet as additional contributors of O, with a stronger metallicity dependence of the O yields (McWilliam et al., 2008).

In the case of Ca, our values are marginally inconsistent with the bulk of field and OC literature determinations. A few literature measurements of OC ratios are however as low as our values. These inconsistencies could be explained with the large uncertainties in the literature loggf values for Calcium lines (~0.2 dex, see discussion in Section 3.1). Given these large additional uncertainties, we finally concluded that [Ca/Fe] is basically compatible with solar values in all the clusters examined.

Concerning Mg, we know already that the log gf values of some lines are still not very well determined (Section 3.1). We also know (Gratton et al., 1999) that some lines require NLTE corrections. We could find no correction factors for the lines we were able to measure in our spectra, but we noticed that those lines examined by Gratton et al. (1999) which have χ_{ex} similar to our lines, require NLTE corrections of about +0.1–0.5 dex. This correction would make our [Mg/Fe] values even higher, reaching an enhancement of 0.2–0.6 dex with respect to solar. Another possibility is that our lines have a non negligible HFS, because they are dominated by odd isotopes, but we could find no further information in the literature. We could only notice that other authors find such relatively high values of [Mg/Fe] in OC (such as Bragaglia et al., 2008).

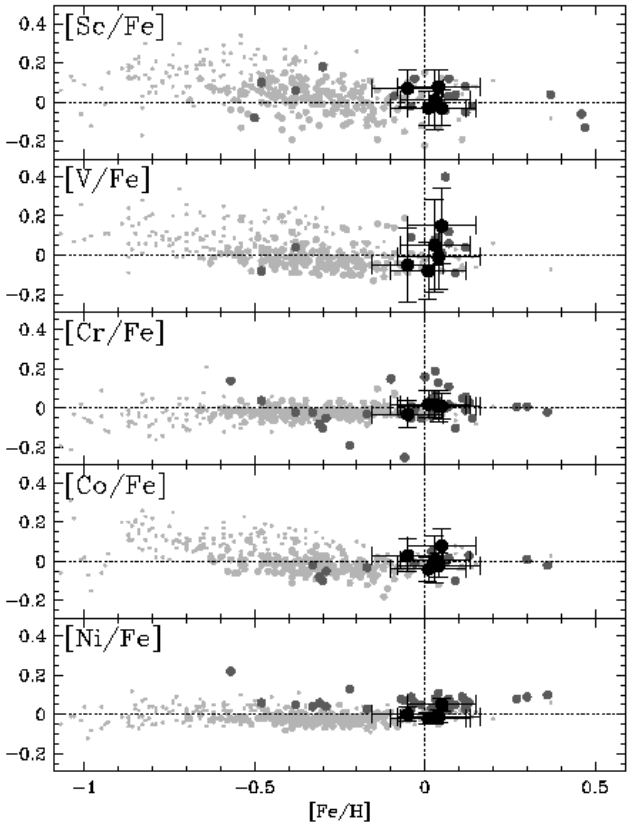

Fig. 4. Comparison between our iron-peak element results (large black dots), the high resolution measurements of other OC listed in Table 13 (large dark grey dots) and field stars belonging to the Thin Disc (light grey dots, Reddy et al., 2003) and to the Thick Disc (tiny light grey dots, Reddy et al., 2006). Errorbars on our results are the quadratic sum of internal uncertainties and uncertainties due to the choice of stellar parameters (Section 4).

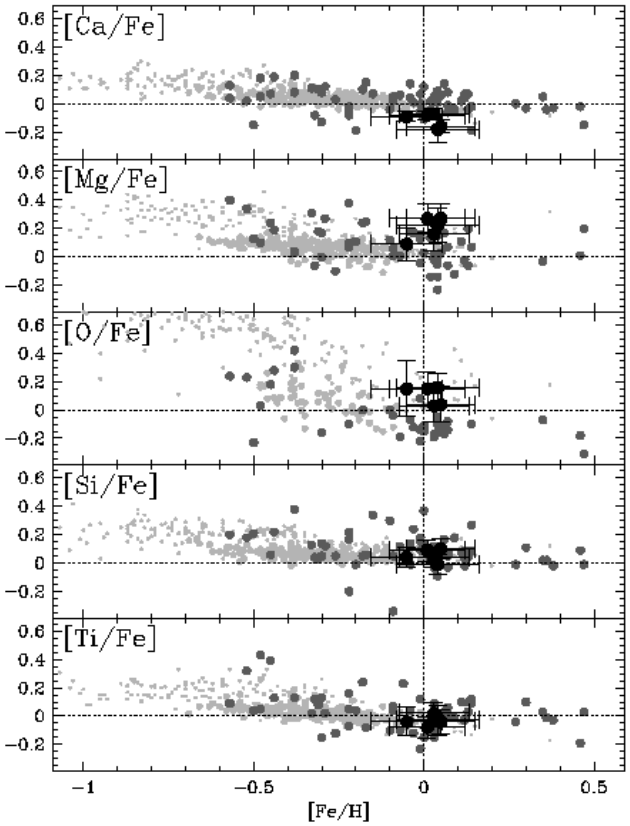

Fig. 5. Comparison between our α-elements ratios and the literature ones. Symbols are the same as in Figure 4.

When the average [α/Fe] values are calculated, however, all the programme stars and the cluster averages appear perfectly compatible with solar, within relatively small uncertainties, as expected (see Tables 7 and 8). The [α/Fe] ratio is also discussed further in Section 7.

6.3. Heavy Elements Ratios

We measured the heavy s-process elements Ba, La and Nd and the light s-process element Y. La does not require any synthesis to take into account HFS, since the three lines we used are always in the linear part of the curve of growth, and in fact Figure 6 shows good agreement with the sparse literature values. Yittrium and neodimium are also in agreement with the literature data, although the measurements of Nd in OC are scarce and scattered. Our values of [Nd/Fe] have a tendency of being towards the upper envelope of the Dics stars, but this is not significant if we consider the large uncertainties involved (see also the discussion in Section 3.2).

Concerning Ba, we find high values both in our programme stars and in the sun itself (Section 4.6). The same result has been found by other authors (e.g., Bragaglia et al., 2008). While a detailed study of the barium abundance is out of the scope of the present paper, we note that very recently D'Orazi et al. (2009) used a detailed HFS analysis of barium in OC and showed that the overabundance can be thus reduced roughly by ∼0.2 dex. Looking at Figure 6, we see that in fact our [Ba/Fe] are on the high side of the OC data, which in turn have a huge spread. Data from D'Orazi et al. (2009), who revised the Ba abundances for 20 OC using spectral synthesis to take HFS into account, are towards the lower envelope of the OC abundances (open stars in Figure 6). As can be seen, some [Ba/Fe] ehnancement remains in their high quality data, that is apparently well correlated with the cluster ages (see their Figure 1). Still no clear explanation is available, since the current evolution models and yields do not reproduce the data correctly at young ages, where the enhancement is higher and more uncertain (up to [Ba/Fe]≃0.6 dex for ages around 10^8). In summary, most of the [Ba/Fe] enhancement we see in our measurements should be due to HFS effects, but some part of it could be real (up to 0.2 dex, see Fig. 2 by D'Orazi et al., 2009). A hint of a descending slope of [Ba/Fe] in OC appears, that is not appaerent among Disc stars. Further studies such as D'Orazi et al. (2009) are necessary on large samples of Disc and OC stars to get firmer constraint on the chemical evolution of Ba in the Galactic Dics.

6.4. Ratios of Na and Al and Anticorrelations

We also derived Na and Al abundances, since these elements are quite easy to measure in OC and there is a vast body of literature measurements to compare with. Figure 7 shows that for

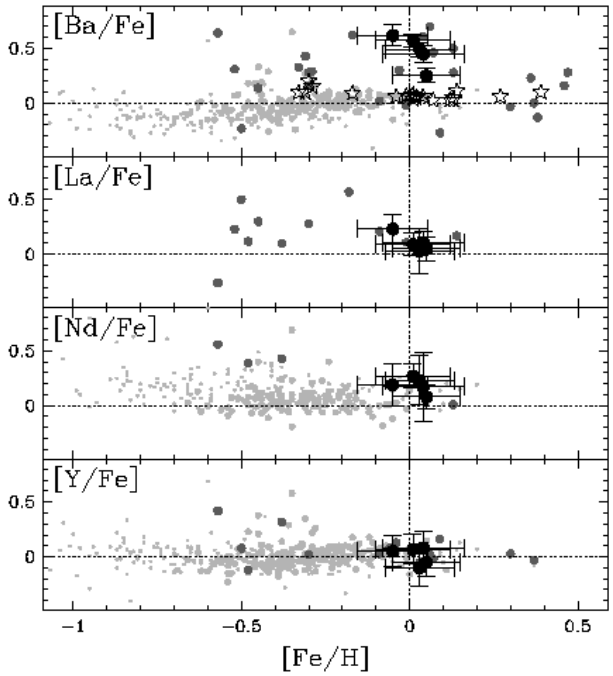

Fig. 6. Comparison between our s-process elements ratios and the literature ones. Symbols are the same as in Figure 4, except for the black star-like symbols in the top [Ba/Fe] panel, which represent the revision of Ba abundances with spectral synthesis performed by D'Orazi et al. (2009).

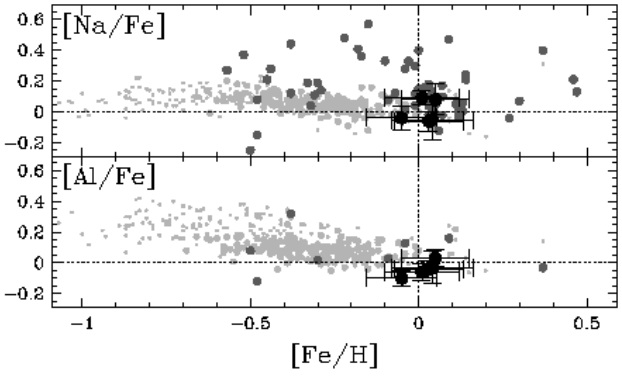

Fig. 7. Comparison between our [Na/Fe] and [Al/Fe] ratios and the literature ones. Symbols are the same as in Figure 4.

Al there is a general agreement between our data, the Disc ratios and the OC ratios, although there is a large scatter in the literature data. NLTE corrections for the four Al doublets and the type of stars studied here could not be found in the literature. Baumüller & Gehren (1997) give corrections for hotter ($T_{\rm eff}$>5000) and higher gravity ($\log g$>3.5) stars, that suggest that either the corrections are negligible, or they are slightly negative at lower temperatures and gravities.

In the case of Na, the spread in the literature data is even larger, and there are both data points with significant Na enhancement and points with typical solar values. Part of the scatter depends on the need for NLTE corrections. According to Gratton et al. (1999), the 5682–5688Å and the 6154–6160Å

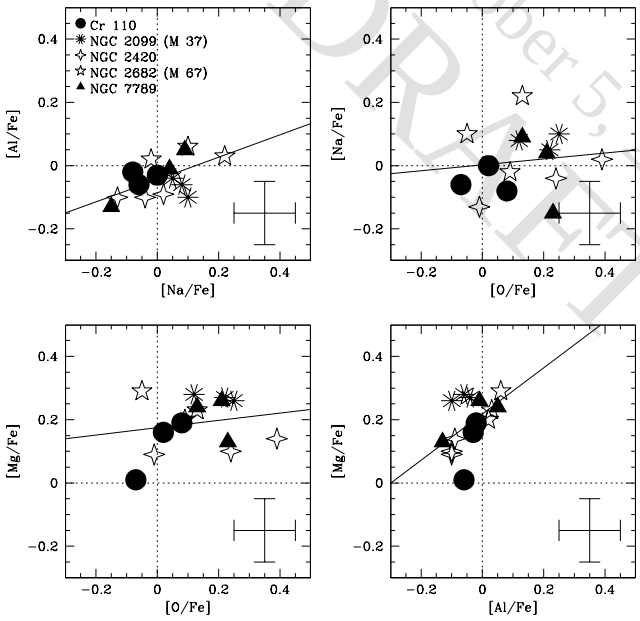

Fig. 8. A search for (anti)-correlations of Al, Mg, Na and O among our targets stars. The four panels show different planes of abundance ratios, where stars belonging to each cluster are marked with different symbols. Dotted lines show solar values, solid lines show linear regressions and the typical uncertainty (~0.1 dex) is marked on the lower right corner of each panel.

doublets at EW≃100 mÅ both require corrections of about ≤0.05–0.10 dex, for solar stars like the ones considered here. The NLTE corrected abundances should be higher than the LTE uncorrected ones: this should make our [Na/Fe] LTE measurements in better agreement with literature measurements. If the observed enhancement in [Na/Fe] should prove to be real for OC, this would set OC stars completely apart form Disc stars (De Silva et al., 2009). If the large spread will also prove to be intrinsic, this would suggest the possibility of light elements chemical anomalies similar, although much less pronounced, to the ones found in Globular Clusters.

In fact Al and Na, together with Mg and O (and C and N) show puzzling (anti)-correlations in almost all of the studied Galactic Globular Clusters (Gratton et al., 2004). The most interesting fact concerning the chemical anomalies, is that they have never been found outside globular clusters. They are not present in the field populations of the Milky Way and its surrounding dwarf galaxies, and they only recently have been found in Fornax and LMC clusters (Letarte et al., 2006; Johnson et al., 2006; Mucciarelli et al., 2009). Recent dedicated searches for anti-correlations in OC are the one by Martell & Smith (2009), on the strength of CH and CN bands in NGC 188, NGC 2158 and NGC 7789, the one by Smiljanic et al. (2008), based on high resolution spectroscopy of C, N, O, Na and $^{12}C/^{13}C$ and the one by De Silva et al. (2009), that compiles and homogenizes literature Na-O high resolution data. No clear-cut sign of anti-correlation has been found yet.

If we build the usual (anti)-correlation plots for our five OC (Figure 8), we find no clear sign of chemical anomalies, and in all four plots the spread of each ratio is still compatible with the typical uncertainty of our measurements, which is of the order of 0.1–0.2 dex, depending on the element. In particular, in

the [O/Fe]–[Na/Fe] plane, all 15 stars roughly occupy the solar region around zero that in Figure 5 by Carretta et al. (2006) contains normal stars only (see also De Silva et al., 2009). A possible exception to this total absence of correlations is the [Na/Fe]–[Al/Fe] plane, where a hint of a correlation can be noticed. Statistically, this is not significant and small variations in T_{eff} could induce a similar weak correlation. For this reason, anti-correlations are usually a more robust sign of chemical anomalies. Still, in light of the discussion by Smiljanic et al. (2008) about the Na-O anti-correlation, our Na-Al results is suggestive. If further studies will show that some chemical anomalies of these elements are present in Galactic OC, our analysis (together with that of Smiljanic et al., 2008) shows that they must be of a much smaller extent than in Globular Clusters: 0.2–0.3 dex at most in the [Al/Fe], [Mg/Fe], [Na/Fe] and [O/Fe] for the kind of clusters studied here. In any case, the lack of relations in OC would point towards one or more of the following environmental causes for the presence of anticorrelations in globular clusters: *(i)* relatively low metallicity (below solar); *(ii)* dense environment; *(iii)* total cluster mass of the order of $\sim 10^4 M_\odot$ or more; *(iv)* undisturbed environment (e.g. away from the Disc, see also Carretta, 2006).

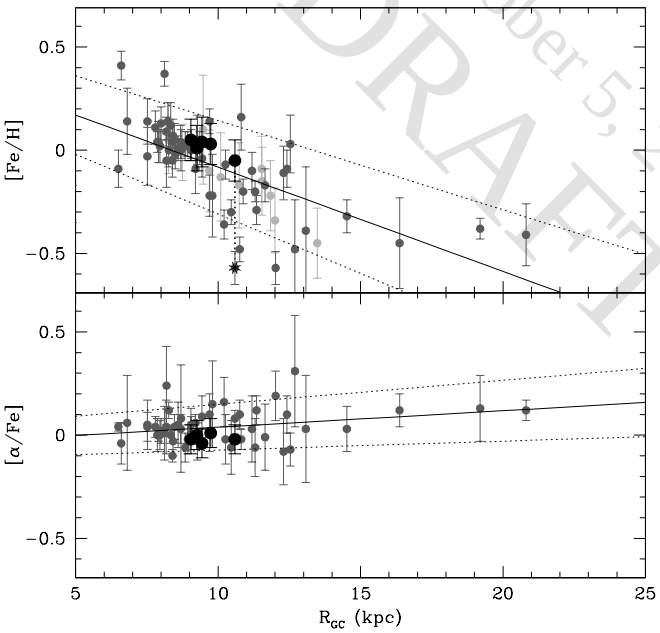

Fig. 9. Trends of [Fe/H] (top panel) and [α/Fe] (bottom panel) with Galactocentric Radius. Light grey dots in the top panel are OC from Friel et al. (2002), grey dots are the OC compiled in Table 13 and black dots are our data. NGC 2420 estimates by us and Smith & Suntzeff (1987) are connected with a thick dotted line. A linear fits with uncertainty is drawn across all points in both panels.

7. Galactic Trends

As said earlier, OC are the fundamental test particles for the study of the chemical evolution of the Galactic Disc, and as such, they produce two of the strongest constraints on chemical models: the Galactic radial trends and the Age-Metallicity Relation (AMR). Since a careful homogeneization of literature data (including not only element ratios, but also ages and Galactocentric radii) is out of the scope of the present paper, we have used the literature data of Table 13, averaging all estimates for a single cluster together. We complemented with data by Friel et al. (2002) for those OC lacking high resolution measurements. Using 28 OC in common between the two datasets, we found an average offset of [Fe/H]=–0.16±0.13 dex, in the sense that the measurements by Friel et al. (2002) are on average smaller than the ones based on high resolution. We corrected Friel et al. (2002) data by this amount before plotting them. We extracted OC ages from the compilation of Dias et al. (2002)[18], and for the Galactocentric Radii (R_{GC}) we used primarily Friel et al. (2002), complemented by the WEBDA, and filled in the few missing clusters with data from the papers of Table 13. The resulting radial trends and AMR for [Fe/H] and [α/Fe] (computed as in Section 4.2) are plotted in Figures 9 and 10 and discussed below.

7.1. Trends with Galactocentric Radius

The trend of abundances with Galactocentric radius R_{GC} gives a strong constraint for the models of Galactic chemical evolution as far as the Disc formation mechanism is concerned[19]. It is now widely accepted (see for example Twarog et al., 1997; Friel et al., 2002; Yong et al., 2005; Sestito et al., 2008; Magrini et al., 2009) that there is a clear trend of decreasing metallicity, measured as [Fe/H], with increasing R_{GC}. Such a trend is clearly detected not only in OC, but also in field stars (B-stars and Cepheids), H II regions and planetary nebulae[20] (see Chiappini et al., 2001; Andrievsky et al., 2004; Yong et al., 2005; Lemasle et al., 2008, for some review of literature data).

The first large studies of homogeneous OC abundances (summarized in the review by Friel, 1995), found that old OC (older than the Hyades) were extending outwards in the Disc, much farther out than young OC, and they found a well defined slope out to $R_{GC} \simeq 16$ kpc. The spread around this slope was at the time around ∼0.2 dex, i.e., generally compatible with (or perhaps slightly larger than) the measurement uncertainties. Such a slope comes naturally in most Galactic chemical evolution models (Tosi, 1982, 1988; Matteucci & Francois, 1989; Tosi, 1996; Chiappini et al., 2001; Andrievsky et al., 2004; Colavitti et al., 2009; Magrini et al., 2009), when different star formation and infall rates are assumed for the inner and outer Disk. To reproduce most of the observational constraints, a differential Disc formation mechanism is often assumed, either with the inner Disk formed first and then growing in radius (inside-out formation) or with the whole Disk evolving simultaneously, but with a much more intense (and sometimes fast) evolution in the central, denser parts. A prediction of all models is that the metallicity gradient should change with time (although different models predict very different time changes, Tosi, 1996) and some predict that it should flatten out at large radii. Indeed, the first studies of anticenter and distant clusters (Carraro et al., 2004; Yong et al.,

[18] We are aware that at least in the case of NGC 6791, the age given by Dias et al. (2002) is quite different from other literature estimates (citations in Tabls 13), being lower by at least 2 Gyr. However, building a homogeneous age scale is a non-trivial task, and it is beyond the scope of the present paper.

[19] A far stronger constraint would be the variation of this trend with age. Such a study is at the moment not possible, given the small number of clusters studied with high resolution in a homogenous way.

[20] Although we know of at leas one dataset in which PNe show flat trends of oxygen and neon abundances with R_{GC} (Stanghellini et al., 2006).

2005; Carraro et al., 2007; Sestito et al., 2008) showed that after $R_{GC}\simeq$12 kpc, the relation flattens around a value of [Fe/H]≃–0.3 dex.

Not much can be said with the present data about the slope variation with time, but the exact value of the slope has been matter of some debate. As said, earlier studies found a value around –0.09±0.01 dex kpc^{-1}, or –0.07±0.01 dex kpc^{-1} with the strictly homogenous measurements by Friel et al. (2002). An alternative interpretation of a different data compilation (Twarog et al., 1997), describes the trend as two disjoint plateaux, one around solar metallicity and comprising OC within R_{GC} ≃10 kpc, and a second one at an [Fe/H]≃–0.3 outside the solar circle. More recent work based on high resolution compilations of OC data (Sestito et al., 2008) find a steeper slope of –0.17±0.01 dex kpc^{-1} within R_{GC} <14 kpc, which still holds when considering only the 10 clusters analyzed homogeneously by that group. A sort of bimodal distribution is observed in their Figure 9, where between the very steep slope of the inner clusters and the plateau of the outer ones there is a small gap almost devoid of OC (9<R_{GC}<12 kpc).

Our results are plotted in Figure 9, where we consider the trend of [Fe/H] and [α/Fe] with R_{GC}. We do see a distinct slope in the inner clusters and a flattening out for the outer ones. However, our sample contains ∼15 more OC than the one of Sestito et al. (2008), and most of them (including our five determinations) fall in the gap around 9<R_{GC}<12 kpc, discussed above. With the addition of these clusters we find a gentler slope of –0.05±0.01 dex kpc^{-1}, in good agreement with previous works (Friel, 1995; Friel et al., 2002) and with the Disk Cepheids within $R_{GC}\simeq$11 kps (Andrievsky et al., 2004; Lemasle et al., 2008). If we exclude the clusters outside R_{GC}=12 kpc and remove the low resolution OC from Friel et al. (2002), the slope does not steepen significantly, becoming –0.06±0.02 dex kpc^{-1}. Also, the flattening out does not seem so abrupt as in Figure 9 by Sestito et al. (2008). The paucity of OC in the flat part of the relation (we have only Be 20, Be 22, Be 29 and Saurer 1 in our compilation) surely calls for more high resolution studies, since as the data stand now, they look compatible with both a plateau and a gradual change in slope. We would like to note that NGC 2420 (already discussed in Section 5.3) was placed at [Fe/H]=–0.57 dex by Smith & Suntzeff (1987), based on R≃16000 spectra, while we find –0.05, in much better agreement with the global Galactic trend. This goes in the direction of filling the gap in the Sestito et al. (2008) compilation, and also in the Twarog et al. (1997) data-set, pointing more towards a gentle and continuous decrease of [Fe/H].

The trend of α-enhancement with R_{GC} is also of some importance, since it unveils the role of SNe type Ia and II and their relative contributions. Yong et al. (2005) found a tendency of the α-enhancement to increase with R_{GC}, as did Magrini et al. (2009), who found this tendency in good agreement with their chemical evolution model. Also model A by Chiappini et al. (2001) predicted an increase of [α/Fe] with R_{GC}. In our compilation, the trend appears as a weak slope, that is still perfectly compatible with a flat distribution at the 1 σ level. This, together with the study of slope changes with time, is one typical case in which a high quality, homogeneous analysis of ∼100 OC could give a clear and definitive answer.

7.2. Trends with Age

In spite of the fact that all models predict an evolution of Disk metallicity with time, albeit maybe only in the first Gyrs, and the fact that such a variation is observed in Disk stars (Reddy et al., 2003; Bensby et al., 2004), there appears to be no correlation at all between old OC abundances and ages (see the review by Friel, 1995). More recent results did not change this picture substantially. If confirmed, the lack of an AMR in OC would point towards a different source of chemical enrichment for OC stars (Yong et al., 2005) with respect to the Disc stars. In substance, the metallicity of OC stars seems to be more determined by the location in which they formed, than by the time at which they formed.

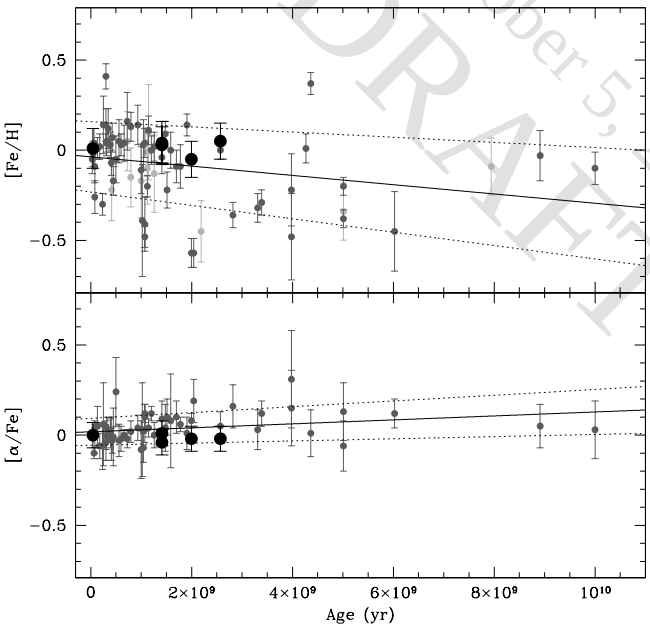

Fig. 10. Trends of [Fe/H] (top panel) and [α/Fe] (bottom panel) with cluster ages. Symbols are the same as in Figure 9.

What we find here is quite encouraging, although still not statistically significant. We recall that our compilation includes 57 high resolution abundance determinations, plus a handful of low resolution determinations by Friel et al. (2002). Although we have made no attempt to homogeneize the data, except for a –0.16 dex correction to the low resolution abundances, this sample is ∼50% larger than any compilation presented before (see e.g., Sestito et al., 2008; De Silva et al., 2009; Magrini et al., 2009) and shows that the community is proceeding fast in filling up the gaps of our knowledge of OC. Figure 10 shows indeed a weak trend of decreasing [Fe/H] and increasing [α/Fe] with increasing age. The slopes are very gentle at best and they are still compatible with no trends at all. Nevertheless, if such trends exist, we can put some constraints on them: for [Fe/H], the gradient should not be significantly larger than –2.6±1.1 10^{-11} dex Gyr^{-1} and for [α/Fe] no larger than 1.1±5.0 10^{-11} dex Gyr^{-1}.

8. Summary and Conclusions

We have analyzed high resolution spectra of three red clump giants in five OC, three of them lacking any previous high resolution based chemical analysis. Given the paucity of literature data, such a small sample is enough to increase the whole body of high resolution data for OC by ≃5%. To compare our results with the literature, we have compiled chemical abundances based on high resolution data of 57 clusters from the literature. Given the recent and fast progress in the field, this sam-

ple is ∼50% larger than previous literature compilations (e.g., Friel et al., 2002; Sestito et al., 2008; Magrini et al., 2009). The main results drawn by the analysis of our five clusters are:

- We provide the first high resolution based abundance analysis of Cr 110 ([Fe/H]=+0.03±0.02 (±0.10) dex), NGC 2099 ([Fe/H]=+0.01±0.05 (±0.10) dex) and NGC 2420 ([Fe/H]=–0.05±0.03 (±0.10) dex), which only had low resolution determinations and the R≃16000 analysis by Smith & Suntzeff (1987); our new determination of the metallicity of NGC 2420 puts this cluster in much better agreement with the global Galactic trends;
- The abundances found for NGC 7789 ([Fe/H]= +0.04±0.07 (±0.10) dex) and M 67 ([Fe/H]= +0.05±0.02 (±0.10) dex) are in good agreement with past high resolution studies;
- We provide the first high resolution based radial velocity determination for Cr 110 (< V_r >=41.0±3.8 km s^{-1});
- We found that all our abundance ratios, with few exceptions generally explained with technical details of the analysis procedure, are near-solar, as is typical for OC with similar properties; we found solar ratios also for Na, that is generally found overabundant, and for O, which is generally found underabundant;
- We do not find any significant sign of anti-correlation (or correlation) among Na, Al, Mg and O, in general agreement with past and recent results, and we can say that if such correlations indeed are present in OC, they must be much less extended than in Globular Clusters, amounting to no more than 0.2–0.3 dex at most;

With our compilation of literature data, we also could examine global Galactic trends, that are extremely useful to construct chemical evolution models for the Galaxy in general and the Galactic Thin Disc in particular. For the metallicity gradient we found a slope of –0.06±0.02 dex kpc^{-1} considering only the high resolution data within R_{GC}=12 kpc. Our compilation contains data, including our own determinations, that fill the small gap around 9<R_{GC} <12 and point towards a gentle and continuous decrease, rather than a two step drop such as in Twarog et al. (1997) or a steep slope such as in Sestito et al. (2008). We do find a flattening at R_{GC} >12 kpc and a hint of an increasing [α/Fe] towards the outer Disk. Concerning the AMR, we do not find any strong evidence for it, and we just note some very mild trends. If an AMR is indeed present among OC, it must be very weak and we provide upper limits to its slope both in [Fe/H] and [α/Fe].

Acknowledgements. We warmly thank A. Bragaglia and A. Mucciarelli for their useful comments and suggestions.We thank M. Tosi and D. Romano for their insights on the chemical evolution modelling of the Milky Way and its Disks. We also warmly thank the Calar Alto Support staff for their hospitality and a good time together. RC, CG and EP acknowledge support by the Spanish Ministry of Science and Technology (Plan Nacional de Investigación Científica, Desarrollo, e Investigación Tecnológica, AYA2004-06343). EP acknowledges support from the Italian MIUR (Ministero dell'Universitá e della Ricerca) under PRIN 2003029437, "Continuities and Discontinuites in the Formation of the Galaxy." RC acknowledges funding by the Spanish Ministry of Science and Innovation under the MICINN/Fullbright post-doctoral fellowship program.

References

Alonso, A., Arribas, S., & Martínez-Roger, C. 1999, A&AS, 140, 261
Andrievsky, S. M., Luck, R. E., Martin, P., & Lépine, J. R. D. 2004, A&A, 413, 159
Arp, H. 1962, ApJ, 136, 66
Andersen, J. 1999, Transactions of the IAU, Vol. XXIVA, p.36 (1999) , 24, A36
Anthony-Twarog B.J., Kaluzny J., Shara M.M., Twarog B.A. 1990, AJ, 99, 1504
Anthony-Twarog, B. J., Tanner, D., Cracraft, M., & Twarog, B. A. 2006, AJ, 131, 461
Aoki, W., et al. 2001, ApJ, 561, 346
Asplund, M., Grevesse, N., & Sauval, A. J. 2005, ASP Conf. Ser. 336: Cosmic Abundances as Records of Stellar Evolution and Nucleosynthesis, 336, 25
Balaguer-Núñez, L., Galadí-Enríquez, D., & Jordi, C. 2007, A&A, 470, 585
Barbaro, G., & Pigatto, L. 1984, A&A, 136, 355
Bartašiutė, S., & Tautvaišienė, G. 2004, Ap&SS, 294, 225
Baumüller, D., & Gehren, T. 1997, A&A, 325, 1088
Bensby, T., Feltzing, S., & Lundström, I. 2004, A&A, 421, 969
Bessell, M. S. 1979, PASP, 91, 589
Boesgaard, A. M., Jensen, E. E. C., & Deliyannis, C. P. 2009, AJ, 137, 4949
Bragaglia, A., et al. 2001, AJ, 121, 327
Bragaglia A., Tosi M. 2003, MNRAS, 343, 306
Bragaglia, A., & Tosi, M. 2006, AJ, 131, 1544
Bragaglia, A., Sestito, P., Villanova, S., Carretta, E., Randich, S., Tosi, M. 2008, A&A, 480, 79
Bramich, D. M., et al. 2005, MNRAS, 359, 1096
Brown, J. A. 1987, ApJ, 317, 701
Brown, J. A., Wallerstein, G., Geisler, D., & Oke, J. B. 1996, AJ, 112, 1551
Bruntt, H., Frandsen, S., Kjeldsen, H., & Andersen, M. I. 1999, A&AS, 140, 135
Burbidge, E. M., & Sandage, A. 1958, ApJ, 128, 174
Burstein, D., Faber, S. M., Gonzalez, J. J., & Spaenhauer, A. 1984, BAAS, 16, 968
Burstein, D., Faber, S. M., & Gonzalez, J. J. 1986, AJ, 91, 1130
Cameron, L. M. 1985, A&A, 147, 39
Cannon R.D., Lloyd C. 1970, MNRAS, 150, 279
Canterna, R., Geisler, D., Harris, H. C., Olszewski, E., & Schommer, R. 1986, AJ, 92, 79
Cardelli, J. A., Clayton, G. C., & Mathis, J. S. 1989, ApJ, 345, 245
Carraro, G. & Chiosi, C. A&A 1994, 287, 761
Carraro, G., Girardi, L., Bressan, A., & Chiosi, C. 1996, A&A, 305, 849
Carraro, G., Bresolin, F., Villanova, S., Matteucci, F., Patat, F., & Romaniello, M. 2004, AJ, 128, 1676
Carraro, G., Villanova, S., Demarque, P., McSwain, M. V., Piotto, G., & Bedin, L. R. 2006, ApJ, 643, 1151
Carraro, G., Geisler, D., Villanova, S., Frinchaboy, P. M., & Majewski, S. R. 2007, A&A, 476, 217
Carrera, R., Gallart, C., Pancino, E., & Zinn, R. 2007, AJ, 134, 1298
Carretta, E., & Gratton, R. G. 1997, A&AS, 121, 95
Carretta, E., Bragaglia, A., Gratton, R. G., & Tosi, M. 2004, A&A, 422, 951
Carretta, E., Bragaglia, A., Gratton, R. G., & Tosi, M. 2005, A&A, 441, 131
Carretta, E., Bragaglia, A., Gratton, R. G., Leone, F., Recio-Blanco, A., & Lucatello, S. 2006, A&A, 450, 523
Carretta, E. 2006, AJ, 131, 1766
Carretta, E., Bragaglia, A., & Gratton, R. G. 2007, A&A, 473, 129
Cayrel de Strobel, G. 1990, Memorie della Societa Astronomica Italiana, 61, 613
Cayrel, R., et al. 2004, A&A, 416, 1117
Chen , L., Hou, J. L. & Wang, J. J. 2003, AJ, 125, 1397
Chiappini, C., Matteucci, F., & Romano, D. 2001, ApJ, 554, 1044
Claria, J. J. 1979, Ap&SS, 66, 201
Clariá, J. J., Mermilliod, J.-C., & Piatti, A. E. 1999, A&AS, 134, 301
Cohen, J. G. 1980, ApJ, 241, 981
Colavitti, E., Cescutti, G., Matteucci, F., & Murante, G. 2009, A&A, 496, 429
Dawson D.W., Ianna P.A. 1995, AJ, 115, 1076
Demarque, P. 1980, Star Formation, 85, 281
Den Hartog, E. A., Lawler, J. E., Sneden, C., Cowan, J. J. 2003ApJS..148..543
De Silva, G. M., Sneden, C., Paulson, D. B., Asplund, M., Bland-Hawthorn, J., Bessell, M. S., & Freeman, K. C. 2006, AJ, 131, 455
De Silva, G. M., Freeman, K. C., Asplund, M., Bland-Hawthorn, J., Bessell, M. S., & Collet, R. 2007, AJ, 133, 1161
De Silva, G. M., Gibson, B. K., Lattanzio, J., Asplund, M. 2009, accepted by A&A Letters, preprint DOI: 10.1051/0004-6361/200912279
Dias, W. S., Alessi, B. S., Moitinho, A., & Lépine, J. R. D. 2002, A&A, 389, 871
Dinescu, D. I., Demarque, P., Guenther, D. B., & Pinsonneault, M. H. 1995, AJ, 109, 2090
Dean, J. F., Warren, P. R., & Cousins, A. W. J. 1978, MNRAS, 183, 569
Demarque, P., Guenther, D. B., & Green, E. M. 1992, AJ, 103, 151
Demarque, P., Sarajedini, A., & Guo, X.-J. 1994, ApJ, 426, 165
D'Orazi, V., Magrini, L., Randich, S., Galli, D., Busso, M., & Sestito, P. 2009, ApJ, 693, L31
Edvardsson, B., Andersen, J., Gustafsson, B., Lambert, D. L., Nissen, P. E., Tomkin, J., 1993, A&A, 275, 101
Fagerholm E. 1906, Uppsala dissertation
Fan X., Burstein D., Chen J.-S., Zhu J., Jlang Z., Wu H., et al. 1996, AJ, 112, 628
Ford, A., Jeffries, R. D., & Smalley, B. 2005, MNRAS, 364, 272
Foy, R., & Proust, D. 1981, A&A, 99, 221
Freeland, E., Deliyannis, C. P., Steinhauer, A., & Sarajedini, A. 2002, Bulletin of the American Astronomical Society, 34, 655

Friel E.D., Janes K.A. 1993 A&A, 267, 75
Friel, E. D. 1995, ARA&A, 33, 381
Friel E.D., Liu T, Janes K.A. 1989 PASP 101, 1105
Friel, E. D., & Boesgaard, A. M. 1992, ApJ, 387, 170
Friel, E. D., Janes, K. A., Tavarez, M., Scott, J., Katsanis, R., Lotz, J., Hong, L., & Miller, N. 2002, AJ, 124, 2693
Friel, E. D., Jacobson, H. R., Barrett, E., Fullton, L., Balachandran, S. C., & Pilachowski, C. A. 2003, AJ, 126, 2372
Friel, E. D., Jacobson, H. R., & Pilachowski, C. A. 2005, AJ, 129, 2725
Frinchaboy, P. M., Marino, A. F., Villanova, S., Carraro, G., Majewski, S. R., & Geisler, D. 2008, MNRAS, 391, 39
Garcia Lopez, R. J., Rebolo, R., & Beckman, J. E. 1988, PASP, 100, 1489
Gebran, M., & Monier, R. 2008, A&A, 483, 567
Geisler, D., Claria, J. J., & Minniti, D. 1991, AJ, 102, 1836
Geisler, D., Claria, J. J., & Minniti, D. 1992, AJ, 104, 1892
Gilliland, R. L., & Brown, T. M. 1992, AJ, 103, 1945
Gim M., Hesser J.E., McClure R.D., Stetson P.B. 1998 PASP, 110, 1172
Gim M., Vandenberg D.A., Stetson P.B., Hesser J.E., Zurek D.R. 1998, PASP, 110, 1318
Girardi, L., & Salaris, M. 2001, MNRAS, 323, 109
Gonzalez, G., & Wallerstein, G. 2000, PASP, 112, 1081
Gratton, R. G., & Contarini, G. 1994, A&A, 283, 911
Gratton, R. G., Carretta, E., Eriksson, K., Gustafsson, B. 1999, A&A, 350, 955
Gratton, R. G., et al. 2001, A&A, 369, 87
Gratton, R. 2000, ASP Conf. Ser. 198: Stellar Clusters and Associations: Convection, Rotation, and Dynamos, 198, 225
Gratton, R., Sneden, C., & Carretta, E. 2004, ARA&A, 42, 385
Grevesse, N., Noels, A., & Sauval, A. J. 1996, ASP Conf. Ser. 99: Cosmic Abundances, 99, 117
Grocholski A. J., & Sarajedini A. 2003, MNRAS, 345, 1015
Hamdani, S., North, P., Mowlavi, N., Raboud, D., & Mermilliod, J.-C. 2000, A&A, 360, 509
Harris, W. E. 1996, AJ, 112, 1487
Hartman, J. D., Gaudi, B. S., Holman, M. J., McLeod, B. A., Stanek, K. Z., Barranco, J. A., Pinsonneault, M. H., & Kalirai, J. S. 2008, ApJ, 675, 1254
Hobbs, L. M., & Thorburn, J. A. 1991, AJ, 102, 1070
Hoffleit, D. & Jaschek, C. —. 1991, New Haven, Conn.: Yale University Observatory, —c1991, 5th rev.ed., edited by Hoffleit, Dorrit; Jaschek, Carlos —v(coll.),
Houdashelt M.L., Frogel J.A., Cohen J.G. 1992, AJ, 103, 163
Jacobson, H. R., Friel, E. D., & Pilachowski, C. A. 2007, AJ, 134, 1216
Jacobson, H. R., Friel, E. D., & Pilachowski, C. A. 2008, AJ, 135, 2341
Jacobson, H. R., Friel, E. D., & Pilachowski, C. A. 2009, AJ, 137, 4753
Jacquinet-Husson, N., Ari, E., Ballard, J., Barbe, A., Bjoraker, G. et al. 1999, JQSRT, 62, 205
Jacquinet-Husson, N., Scott, N. A., Garceran, K., Armante, R., Chédin, A. 2005, JQSRT, 95, 429
Jahn, K., Kaluzny, J., & Rucinski, S. M. 1995, A&A, 295, 101
Janes, K. A. 1977, AJ, 82, 35
Janes, K. A. 1979, ApJS, 39, 135
Janes K.A., Smith G.H. 1984, AJ, 89, 487
Janes, K. A., Tilley, C., & Lynga, G. 1988, AJ, 95, 771
Janes, K. A., & Phelps, R. L. 1994, AJ, 108, 1773
Jennens, P. A., & Helfer, H. L. 1975, MNRAS, 172, 681
Johansson, S., Litzén, U., Lundberg, H., & Zhang, Z. 2003, ApJ, 584, L107
Johnson, J. A., Ivans, I. I., & Stetson, P. B. 2006, ApJ, 640, 801
Jones, B. F., Fischer, D., & Soderblom, D. R. 1999, AJ, 117, 330
Kinman, T., & Castelli, F. 2002, A&A, 391, 1039
Kalirai J.S., Ventura P., Richer H.B., Fahlman G.G., Durrell P.R., D'Antona F., Marconi G. 2001, AJ, 122, 3239
Kalirai, J. S., & Tosi, M. 2004, MNRAS, 351, 649
Kiss L.L., Szabo Gy., Sziladi K., Furesz G., Sarneczky K., Csak B. 2001, A&A, 376, 561
Kraft, R. P., & Ivans, I. I. 2003, PASP, 115, 143
Kupka, F., Piskunov, N., Ryabchikova, T. A., Stempels, H. C., & Weiss, W. W. 1999, A&AS, 138, 119
Kustner K. 1923, Veroeff. Univ. Sternw., Bonn no 18
Lasker B.M., Russel J.N., Jenkner H., Sturch C.R., McLean B.J., Shara M.M. 1990, AJ, 99, 2019
Lattanzio, J. C. 1984, MNRAS, 207, 309
Laugalys, V., Kazlauskas, A., Boyle, R. P., Vrba, F. J., Davis Philip, A. G. & Straižys, V. 2004, Baltic Astronomy, 13, 1
Lemasle, B., François, P., Piersimoni, A., Pedicelli, S., Bono, G., Laney, C. D., Primas, F., & Romaniello, M. 2008, A&A, 490, 613
Letarte, B., Hill, V., Jablonka, P., Tolstoy, E., François, P., & Meylan, G. 2006, A&A, 453, 547
Liu T., Janes K.A. 1987, PASP, 99, 1076
Lyngå, G. 1987, European Regional Astronomy Meeting of the IAU, Volume 4, 4, 121
Magain, P. 1984, A&A, 134, 189
Magrini, L., Sestito, P., Randich, S., & Galli, D. 2009, A&A, 494, 95
Marshall, J. L., Burke, C. J., DePoy, D. L., Gould, A., & Kollmeier, J. A. 2005, AJ, 130, 1916
Martell, S. L., & Smith, G. H. 2009, arXiv:0905.3175
Martinez Roger, C., Paez, E., Castellani, V., & Straniero, O. 1994, A&A, 290, 62
Mathieu R.D., Latham D.W., Griffin R.F., Gunn J.E. 1986, AJ, 92, 1100
Matteucci, F., & Francois, P. 1989, MNRAS, 239, 885
Mazzei, P., & Pigatto, L. 1988, A&A, 193, 148
McClure, R. D., Forrester, W. T., & Gibson, J. 1974, ApJ, 189, 409
McClure, R. D., Newell, B., & Barnes, J. V. 1978, PASP, 90, 170
McNamara, B. J. 1980, PASP, 92, 682
McWilliam, A., Preston, G. W., Sneden, C., & Searle, L. 1995, AJ, 109, 2757
McWilliam, A., Matteucci, F., Ballero, S., Rich, R. M., Fulbright, J. P., & Cescutti, G. 2008, AJ, 136, 367
Melo C.H.F., Pasquini L., De Medeiros J.R. 2001, A&A, 375, 851
Mermilliod, J.-C. 1995, ASSL Vol. 203: Information & On-Line Data in Astronomy, 127
Mermilliod, J.-C., Huestamendia, G., del Rio, G., Mayor, M. 1996, A&A, 307, 80
Mermilliod, J. C., Mayor, M., & Udry, S. 2008, A&A, 485, 303
Meynet, G., Mermilliod, J.-C., & Maeder, A. 1993, A&AS, 98, 477
Milone, A. A. E., & Latham, D. W. 1994, AJ, 108, 1828
Mochejska B.J., Kaluzny J. 1999, Acta Astron., 49, 351
Montegriffo, P., Ferraro, F. R., Origlia, L., & Fusi Pecci, F. 1998, MNRAS, 297, 872
Montgomery, K. A., Marschall, L. A., & Janes, K. A. 1993, AJ, 106, 181
Moore, C. E., Minnaert, M. G. J., & Houtgast, J. 1966, National Bureau of Standards Monograph, Washington: US Government Printing Office (USGPO)
Mucciarelli, A., Origlia, L., Ferraro, F. R., & Pancino, E. 2009, ApJ, 695, L134
Nilakshi, Sagar R. 2002, A&A, 381, 65
Nissen, P. E., Twarog, B. A., & Crawford, D. L. 1987, AJ, 93, 634
Origlia, L., Valenti, E., Rich, R. M., & Ferraro, F. R. 2006, ApJ, 646, 499
Pace, G., Pasquini, L., & François, P. 2008, A&A, 489, 403
Panagia, N., & Tosi, M. 1980, A&A, 81, 375
Pasquini, L., Randich, S., & Pallavicini, R. 1997, A&A, 325, 535
Pasquini, L., Randich, S., Zoccali, M., Hill, V., Charbonnel, C., & Nordström, B. 2004, A&A, 424, 951
Pasquini, L., Biazzo, K., Bonifacio, P., Randich, S., & Bedin, L. R. 2008, A&A, 489, 677
Paulson, D. B., Sneden, C., & Cochran, W. D. 2003, AJ, 125, 3185
Pilachowski, C. A., Wallerstein, G., & Canterna, R. 1980, ApJ, 235, L21
Pilachowski, A. A. 1985, PASP, 97, 801
Peterson, R. C., & Green, E. M. 1998, ApJ, 502, L39
Pilachowski, C. 1986, ApJ, 300, 289
Pilachowski C.A., Saha A., Hobbs L.M. 1988, PASP, 100, 474
Plez, B., Brett, J. M., & Nordlund, A. 1992, A&A, 256, 551
Pols, O. R., Schroder, K.-P., Hurley, J. R., Tout, C. A., & Eggleton, P. P. 1998, MNRAS, 298, 525
Prochaska, J. X., & McWilliam, A. 2000, ApJ, 537, L57
Racine, R. 1971, ApJ, 168, 393
Ramírez, S. V., & Cohen, J. G. 2003, AJ, 125, 224
Randich, S., Pallavicini, R., Meola, G., Stauffer, J. R., & Balachandran, S. C. 2001, A&A, 372, 862
Randich, S., Sestito, P., & Pallavicini, R. 2003, A&A, 399, 133
Randich, S., Sestito, P., Primas, F., Pallavicini, R., & Pasquini, L. 2006, A&A, 450, 557
Randich, S., Primas, F., Pasquini, L., Sestito, P., & Pallavicini, R. 2007, A&A, 469, 163
Reddish, V. C. 1954, MNRAS, 114, 583
Reddy, B. E., Tomkin, J., Lambert, D. L., & Allende Prieto, C. 2003, MNRAS, 340, 304
Reddy, B. E., Lambert, D. L., & Allende Prieto, C. 2006, MNRAS, 367, 1329
Rutten, R. J., van der Zalm, E. B. J. 1984, A&AS, 55, 171
Salaris, M., Cassisi, S. 1998, MNRAS, 298, 166
Salaris, M., Weiss, A., & Percival, S. M. 2004, A&A, 414, 163
Sandquist E.L. 2004, MNRAS, 347, 101
Santos, N. C., Lovis, C., Pace, G., Melendez, J., & Naef, D. 2009, A&A, 493, 309
Sarajedini, A. 1999, AJ, 118, 2321
Sarma, M. B. K., & Walker, M. F. 1962, ApJ, 135, 11
Schönberner, D., Andrievsky, S. M., & Drilling, J. S. 2001, A&A, 366, 490
Schuler, S. C., King, J. R., Fischer, D. A., Soderblom, D. R., & Jones, B. F. 2003, AJ, 125, 2085

Scott J.E., Friel E.D., Janes K.A. 1995, AJ, 109, 1706
Sestito, P., Randich, S., Mermilliod, J.-C., & Pallavicini, R. 2003, A&A, 407, 289
Sestito, P., Randich, S., & Bragaglia, A. 2007, A&A, 465, 185
Sestito, P., Bragaglia, A., Randich, S., Pallavicini, R., Andrievsky, S. M., & Korotin, S. A. 2008, A&A, 488, 943
Shetrone, M. D., & Sandquist, E. L. 2000, AJ, 120, 1913
Skrutskie, M. F., et al. 2006, AJ, 131, 1163
Smiljanic, R., Gauderon, R., North, P., Barbuy, B., Charbonnel, C., & Mowlavi, N. 2008, arXiv:0810.1701
Spite, M. 1967, Annales d'Astrophysique, 30, 211
Steffen, M. 1985, A&AS, 59, 403
Smith, V. V., & Suntzeff, N. B. 1987, AJ, 93, 359
Stanghellini, L., Guerrero, M. A., Cunha, K., Manchado, A., & Villaver, E. 2006, ApJ, 651, 898
Stetson, P. B. 1987, PASP, 99, 191
Stetson P.B. 2000, PASP, 112, 925
Stetson, P. B., & Pancino, E. 2008, PASP, 120, 1332
Strom, K. M., & Strom, S. E. 1970, ApJ, 162, 523
Suntzeff N.B., Schommer R.A., Olzewski E.W., Walker A.R. 1992, AJ, 104, 1743
Tadross, A. L., Werner, P., Osman, A., & Marie, M. 2002, New Astronomy, 7, 553
Tautvaišiene, G., Edvardsson, B., Tuominen, I., Ilyin, I. 2000, A&A, 360, 499
Tautvaišienė, G., Edvardsson, B., Puzeras, E., & Ilyin, I. 2005, A&A, 431, 933
Tiede, G. P., Martini, P., & Frogel, J. A. 1997, AJ, 114, 694
Tosi, M. 1982, ApJ, 254, 699
Tosi, M. 1988, A&A, 197, 47
Tosi, M. 1996, From Stars to Galaxies: the Impact of Stellar Physics on Galaxy Evolution, 98, 299
Tsarevskii G. S., Abakumov I. E. 1971, Astron. Tsirk., 631, 6
Twarog, B. A., & Tyson, N. 1985, AJ, 90, 1247
Twarog, B. A., Ashman, K. M., & Anthony-Twarog, B. J. 1997, AJ, 114, 2556
Twarog, B. A., Anthony-Twarog, B. J., & De Lee, N. 2003, AJ, 125, 1383
Vallenari, A., Carraro, G., & Richichi, A. 2000, A&A, 353, 147
van Altena, W. F., & Jones, B. F. 1970, A&A, 8, 112
Vandenberg, D. A. 1985, ApJS, 58, 711
VandenBerg, D. A., & Clem, J. L. 2003, AJ, 126, 778
van Zeipel H., Lindgren J. 1921, Kungl. Sven. Vet. Handl. 61 no 15
Villanova, S., Carraro, G., Bresolin, F., & Patat, F. 2005, AJ, 130, 652
Villanova, S., Baume, G., & Carraro, G. 2007, MNRAS, 379, 1089
Warren, S. R., & Cole, A. A. 2008, arXiv:0811.2925
West, F. R. 1967, Publications of the Goethe Link Observatory, 75, 359
West, F. R. 1967, ApJS, 14, 384
Yadav, R. K. S., et al. 2008, A&A, 484, 609
Yong D., Carney B.W., Texeira de Almeida M.L. 2005, AJ, 130, 597
Zinn, R., & West, M. J. 1984, ApJS, 55, 45